Transport Canada airborne detect and avoid flight trials 2022/2023

Ellis, Kris; Jennings, Sion

Publisher's version / Version de l'éditeur:
https://doi.org/10.4224/40003222
Laboratory Technical Report (National Research Council of Canada. Flight Research Laboratory); no. LTR-FRL-2024-003, 2024-01-23

NRC·CNRC *Flight Research – Aerospace Research Centre*

Transport Canada Airborne Detect and Avoid Flight Trials 2022/2023

LTR-FRL-2024-003

23 January 2024

Authors/Auteurs : **Kris Ellis, Sion Jennings**

National Research Council Canada | Conseil national de recherches Canada

Canada

FLIGHT RESEARCH LABORATORY

Transport Canada Airborne Detect and Avoid Flight Trials 2022/2023

Report No.: LTR-FRL-2024-003

Date: 23 January 2024

Authors/Auteurs: Kris Ellis, Sion Jennings

Classification :	Unclassified	**Distribution :**	Unlimited
For:			
Reference:			
Submitted by:			
Approved by:	Heather Wright Beatty, **Director Flight Research Laboratory (Acting)**		

Pages : 78
Fig. : 44

ABSTRACT

Transport Canada (TC) and NRC have identified several key areas of technology performance evaluation that are required to enable safe Remotely Piloted Aircraft System (RPAS) operations conducted Beyond Visual Line of Sight (BVLOS); a key area that has been identified is RPAS detect and avoid (DAA) capability. Advancing technology performance assessment in this area will help guide operational risk assessments for future BVLOS SFOC applications as well as inform regulatory developments.

In 2020 TC, LookNorth, and NRC conducted an initial investigation into operator/integrator developed ground based DAA systems that involved the operators conducting flight tests of their systems, and providing the data to NRC for analysis. The results published in 2021indicated a desire to improve the consistency of data collection and test design, as well as to collect more data regarding airborne DAA systems.

As a result, TC performed a targeted call for participation to industry, which targeted technologies/systems with detection technology onboard of the Remotely Piloted Aircraft (RPA). This project differs from the previous DAA evaluation project (LookNorth/TC 2021), as mounting each DAA system onboard a single traditional aircraft ensured known and common test conditions.

National Research Council Canada and Transport Canada obtained participation from 3 airborne DAA system manufacturers with different sensor modalities (1 electro-optical and 2 radar-based). The selected systems were integrated onto the NRC Bell 205 airborne simulator medium utility helicopter, and a series of 80 flight test points were conducted using the NRC Mk IV Harvard, and Bell 206 Jetranger as instrumented Intruder aircraft.

This report provides an overview of each of the systems tested including a description of the hardware and software integration of the DAA systems on board the NRC Bell 205 as well as the supporting systems developed to facilitate the conduct of ‘near miss intercepts’. An overview of the flight test plan, the associated techniques, and the test objectives is then provided. Next, the report breaks out the integration and test performance aspects of the individual systems. Finally, the combined system performance is presented followed by conclusions and recommendations.

None of the sensors tested can be considered as complete ‘plug-and-play’ systems. The task of having to integrate three sensors to a single airborne platform highlighted the fact that there is no common interface standard definition for DAA sensors. Moreover, the three sensors tested required different degrees of integration and levels of familiarity with the basic sensing modality and its associated parameters.

All sensors exhibited average detection ranges that were comparable with the manufacturer’s published specifications, however the variance between intercepts was significant. It is conjectured that this variance will have an impact on the realized risk ratio of the DAA system. The range at first detection performance achieved for the closing rates tested yielded a time to closest approach of 20 to 40 seconds on average. These values are low if the decision making loop requires human intervention. If the DAA system requires human intervention, the delay times should be accounted for in any modelling effort used to assess the full system risk ratio.

The salient conclusion from this flight testing is that the performance results are highly dependent on the quality of the system integration. Moreover, one cannot conduct a performance assessment of the sensor alone without considering the integration into the greater system. The importance of flight testing DAA systems for RPAs cannot be overstated, as it is the ultimate validation of functionality and effectiveness of these systems in real-world scenarios, allowing both the operator and regulator to understand the degree to which DAA systems can mitigate the air risk. The airborne testing of three DAA sensors described in this

report highlights the importance of flight testing for both system performance validation as well as system integration testing and development. Each integration of a DAA sensor into a specific RPAS and airspace (i.e. traffic distribution) will require a separate assessment of risk ratio. This highlights the need for a well established and agreed upon means for integrators to calculate the risk ratio.

RESUME

Transports Canada (TC) et le CNRC ont identifié plusieurs domaines clés d'évaluation du rendement technologique qui sont nécessaires pour permettre des opérations sécuritaires de systèmes d'aéronefs télépilotés (RPAS) menées au-delà de la ligne de visée visuelle (BVLOS); en particulier la capacité de détection et d'évitement des RPAS (DAA). Faire progresser l'évaluation des performances technologiques dans ce domaine aidera à orienter les évaluations des risques opérationnels pour les futures applications BVLOS SFOC ainsi qu'à éclairer les évolutions réglementaires.

Par conséquent, TC a lancé un appel à participation ciblé auprès de l'industrie, ciblant les technologies/systèmes dotés d'une technologie de détection à bord des aéronefs télépilotés (RPA). Ce projet diffère du précédent projet d'évaluation DAA (LookNorth/TC 2021), car le montage de chaque système DAA à bord d'un seul avion traditionnel garantissait des conditions de test connues et communes.

Le Conseil national de recherches Canada et Transports Canada ont obtenu la participation de trois fabricants de systèmes DAA aéroportés dotés de différentes modalités de capteurs (1 électro-optique et 2 basés sur un radar). Les systèmes sélectionnés ont été intégrés sur l'hélicoptère utilitaire moyen simulateur aéroporté Bell 205 du CNRC, et une série de 80 points d'essai en vol ont été effectués en utilisant le Harvard Mk IV du CNRC et le Bell 206 Jetranger comme avions Intruder instrumentés.

Ce rapport donne un aperçu de chacun des systèmes testés, y compris une description de l'intégration matérielle et logicielle des systèmes DAA à bord du Bell 205 du CNRC ainsi que des systèmes de soutien développés pour faciliter la réalisation d'interceptions évitées de justesse. Un aperçu du plan de test en vol, des techniques associées et des objectifs du test est ensuite fourni. Ensuite, le rapport détaille les aspects d'intégration et de performances de test des systèmes individuels. Enfin, les performances combinées du système sont présentées, suivies de conclusions et de recommandations.

Aucun des capteurs testés ne peut être considéré comme un système complet « plug-and-play ». La tâche consistant à devoir intégrer trois capteurs sur une seule plate-forme aéroportée a mis en évidence le fait qu'il n'existe pas de définition standard d'interface commune pour les capteurs DAA. De plus, les trois capteurs testés nécessitaient différents degrés d'intégration et niveaux de familiarité avec la modalité de détection de base et ses paramètres associés.

Tous les capteurs présentaient des plages de détection moyennes comparables aux spécifications publiées par le fabricant, mais la variance entre les interceptions était significative. On suppose que cet écart aura un impact sur le rapport de risque réalisé du système DAA. La plage de performances de première détection obtenue pour les taux de fermeture testés a donné un temps jusqu'à l'approche la plus proche de 20 à 40 secondes en moyenne. Ces valeurs sont faibles si la boucle de prise de décision nécessite une intervention humaine. Si le système DAA nécessite une intervention humaine, les délais doivent être pris en compte dans tout effort de modélisation utilisé pour évaluer le rapport de risque complet du système.

La principale conclusion de ces essais en vol est que les résultats en matière de performances sont directement liés aux efforts d'intégration du système. De plus, on ne peut pas évaluer les performances du capteur seul sans considérer son intégration dans le système global. Cela signifie que chaque intégration d'un capteur DAA dans un RPAS et un espace aérien spécifiques (c'est-à-dire la répartition du trafic) nécessitera une évaluation distincte du rapport de risque. Cela met en évidence la nécessité de disposer de moyens bien établis et convenus permettant aux intégrateurs de calculer le rapport de risque.

TABLE OF CONTENTS

LIST OF FIGURES

LIST OF TABLES

NOMENCLATURE

AGL	Above Ground Level
ASTM	American Society for Testing Materials
ATC	Air Traffic Control
ARC (A-D)	Air Risk Class (A – D)
AWGN	Average White Gaussian Noise
CARAC	Canadian Aviation Regulatory Advisory Council
CFAR	Constant False Alarm Rate
CSV	Comma Separated Value
CV	Computer Vision
DAA	Detect and Avoid
FFT	Fast Fourier Transform
FLIR	Forward looking Infrared
FRL	Flight Research Laboratory
GBDAA	Ground Based Detect and Avoid
GMT	Greenwich Mean Time
GPS	Global Positioning System
HPBW	Half Power Beam Width
IMU	Inertial Measurement Unit
INS	Inertial Navigation System
IMM	Interacting Multiple Model
IP	Initial Point
JARUS	Joint Authorities for Rulemaking on Unmanned Systems
KIAS	Knots Indicated Airspeed
LED	Light Emitting Diode
MDS	Minimum Detectable Signal
MEMS	Micro Electro-Mechanical Systems
NM	Nautical Mile
NRC	National Research Council
OGD	Other Government Departments
OEM	Original Equipment Manufacturer
PDF	Probability Density Function
PPI	Plan Position Indication
PPS	Pulse Per Second
PRF	Pulse Repetition Frequency
QGC	Q-Ground Control
RCS	Radar Cross Section
RPA	Remotely Piloted Aircraft
RPAS	Remotely Piloted Aircraft System
RTB	Return to Base
SFTP	Secure File Transfer Protocol
SNR	Signal to Noise Ratio
SORA	Specific Operations Risk Assessment
TC	Transport Canada
TPSI	Time Space Positioning Information
TTG	Time To Go
UAS	Unmanned Aircraft System
UDP	Universal Datagram Packet
UTC	Universal Coordinated Time

UTM	Universal Trans Mercator
VLOS	Visual Line of Sight

1.0 BACKGROUND

The proliferation of remotely piloted aircraft (RPA), has led to an increased need for detect and avoid (DAA) systems. These systems are critical for ensuring the safe operation of RPAs in airspace shared with traditional aircraft. DAA systems are still a developing technology, and as such the performance standards, regulations are evolving with the technology itself. Transport Canada is allowing for limited Beyond Visual Line of Sight (BVLOS) flight approvals under the Specific Operations Risk Assessment (SORA) process, which requires the operator to demonstrate how their concept of operations and systems mitigate the risks to an acceptable level. The importance of flight testing DAA systems for RPAs cannot be overstated, as it is the ultimate validation of functionality and effectiveness of these systems in real-world scenarios, allowing both the operator and regulator to understand the degree to which DAA systems can mitigate the risk of midair collision with other users of the airspace.

DAA systems use a combination of sensors, algorithms, and communication links to detect and avoid potential collisions with other aircraft. These systems are critical for ensuring the safe operation of RPAs, particularly in situations where the pilot may be operating the vehicle remotely and may not have a clear view of the airspace. Flight testing DAA systems allows researchers and regulators to evaluate the performance of the sensors and algorithms in real-world scenarios, which is crucial for ensuring that the systems work as intended and can effectively prevent collisions.

Another important aspect of flight testing DAA systems is the opportunity to identify potential limitations and areas for improvement. Flight testing allows researchers to collect data on the performance of the systems in various scenarios, including different weather conditions and types of traffic. This data can then be used to refine the algorithms and sensors, as well as to develop new technologies that can enhance the effectiveness of the DAA systems.

Flight testing also allows researchers to better understand issues related to the integration of DAA systems with the rest of the RPAS. Integrating DAA systems with other components of the RPAS can be complex and challenging, and flight testing provides an opportunity to assess how well the different systems work together. This includes evaluating the impact of DAA systems on the overall performance of the RPAS, as well as any potential conflicts or issues that may arise during operation.

The National Research Council Canada has established a technology demonstration and development program in the area of RPAS, with the objective of advancing RPAS technologies to foster higher economic activities in Canada. Through this initiative, NRC has consulted with and engaged the stakeholders and end-users in various industries, Other Government Departments (OGD) and aerospace Original Equipment Manufacturers (OEM). The program addresses the technology gaps while at the same time engages with the end-user industry to streamline the activities for a higher impact. NRC has been a regular contributor to the Canadian Aviation Regulatory Advisory Council (CARAC) and participated in the TC UAV Program Design working group at both the main and subgroup levels.

NRC has partnered with several government organizations (e.g., Canadian Coast Guard, Royal Canadian Navy, Correctional Services Canada, etc.) to conduct state-of-the art analysis and technical evaluation of the UAS/RPAS technologies for the applications in the clients' targeted operations. In 2018 NRC's Flight Research Laboratory conducted trials and analysis of the Seamatica Aerospace Ltd 'GuardianEye' ground based detect and avoid system (References 1-3). This testing established vital experience regarding the development of test methods for ground based Detect and Avoid systems, and leveraged FRL's considerable experience with the testing of airborne systems (Reference 4).

In 2019 TC announced a call for proposals to investigate DAA enabling technologies via flight test. Two Canadian companies (proponents) were selected to demonstrate their systems via flight test:

1. Canadian UAV's (ground based radar system)
2. Pegasus (air based radar system – tested on ground)

Reference 5 presented the flight test data and analysis of the two developmental radar based detect and avoid systems. Both systems showed significant potential for use in RPAS operations BVLOS, however further development and testing was recommended prior to conducting operations in Air Risk Class ARC-C airspace. A further conclusion from the trial was that the lack of consistency in test approach made it difficult to compare the performance of the systems, and the inability to conduct testing in a 'build-up' approach precluded the ability to implement minor fixes that would have improved the data consistency and quality.

In 2021 Transport Canada announced its intention to collect performance data on particular airborne DAA systems that they expected to see referenced in applications for BVLOS operations. To this end Transport Canada sought to better understand the performance capabilities of these systems as well as the integration aspects that would need to be performed by the system integrator. TC performed a targeted call for participation to industry, which targeted technologies/systems with detection technology onboard of the Remotely Piloted Aircraft (RPA). The three systems selected for evaluation were:

1. Iris Automation Casia X – Electro/Optical
2. Echodyne EchoFlight – Radar
3. Fortem Technologies R20i – Radar

To improve upon the lessons learned from the TC/LookNorth Trial it was decided to integrate all three selected systems on the NRC's Bell 205 Airborne Simulator medium helicopter serving as a surrogate RPA, and to employ instrumented NRC aircraft as intruders. This approach was selected as it effectively tripled the data output, and allowed for improved comparison of the systems under common operating and target conditions.

2.0 SYSTEMS UNDER TEST

The DAA (Detect and Avoid) camera/radar systems were mounted under the nose of the NRC Bell 205 and on the FLIR mount of the Bell 205. The radar and camera sensor installations are shown in Figure 1-3 while the associated power switches on the crew workstation rack are shown in Figure 4. Further details regarding NRC drawing numbers (in the format YZV####) and installation modification cards are below.

a) The radar mounting frame consisting of the existing Chin Mount Assy (YZV09021), Interface Rail (YZV11040), Interface Plate (YZV17004), and Seamatica Radar Mount Assy (YZV17006) to mount radars.;
b) Echodyne EchoFlight DAA Radar (700-0005-201-100) looking forward and rotated 40° towards port. With a 120° FOV, this allows the radar to see 20° towards starboard;
c) Fortem Trueview Radar (R20i) looking forward and rotated 40° towards port. With a 120° FOV, this allows the radar to see 20° towards starboard;
d) Existing forward/port side FLIR mount (412-706-041-101) to mount camera
e) Two Casia X DAA cameras (HEOC-0009) looking forward and rotated towards port with overlapping camera angles to cover the same field of view as the radars;
f) Casia X DAA processor module (XACM-0100) on a shelf in the NRC Bell 205 ADS-B Client Rack, and;
g) Power switches for each radar accessible at the engineering workstation (Figure 5), which are controlled through the main project power switch in the cockpit.

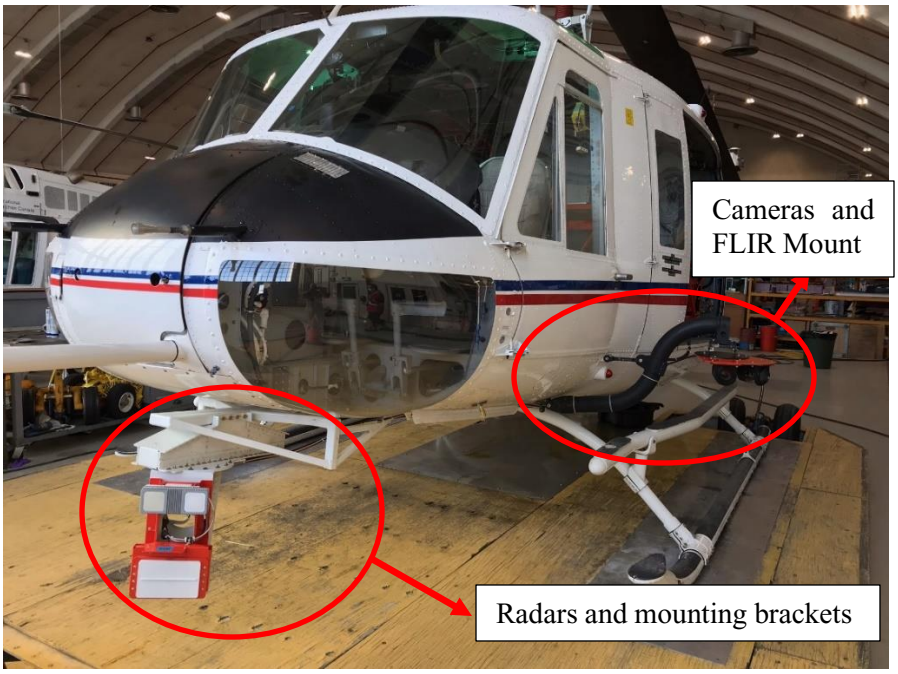

Figure 1: Detect and Avoid Sensors on Bell 205

Figure 2: CASIA Camera Module (L) and CASIA Cameras on FLIR Mounting Arm (R)

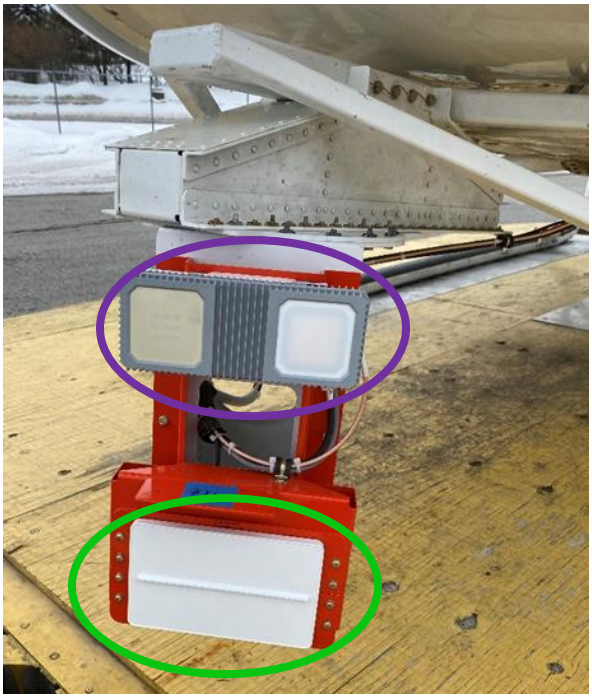

Figure 3: EchoDyne Echoflight (green ellipse) and Fortem Technologies R20i (purple ellipse)

Figure 4: Engineering Workstation power switches

The intruder aircraft were temporarily modified with the installation of a "seated man rack" which contained a computer and an ADS-B transceiver and is shown in Figure 5. In both the Bell 206 and the Harvard the unit was strapped into the rear seat.

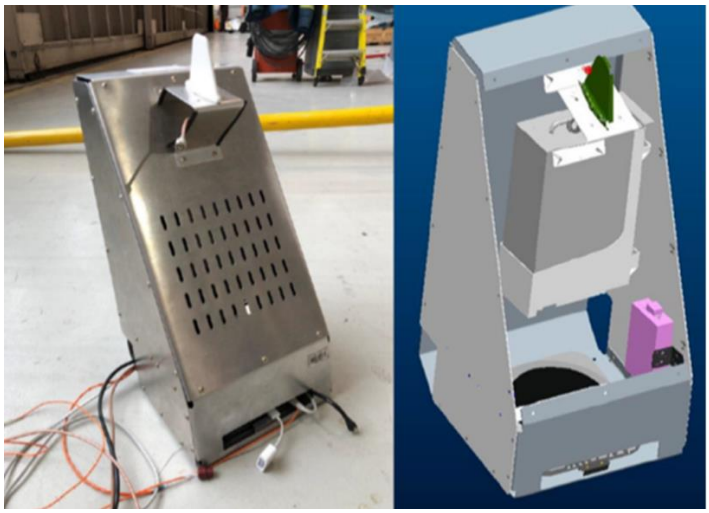

Figure 5: Seated Man Rack

Each of the flight test aircraft serving as an intruder had a temporary fitting of an iPhone 12 that displayed the NRC iCollide guidance. The iCollide software was pre-configured for a single ground speed, thus all high altitude intercepts using the display were flown at a constant speed for each intruder. The collision guidance was based on ground speeds and flown to a pre-selected conflict point. Since the sorties were

flown on ground speed, a safety margin above the stall speed was required to accommodate the effects of winds on the aircraft airspeed.

The Detect and Avoid sensors were interfaced to the Bell 205 Engineering Workstation for central collection of data in the standard FRL file format. Supporting displays were developed/configured in the Bell 205, as shown in Figure 6 (higher quality images of the displays are available later in the report). The left display is located at the Evaluation Pilot position, and provides situational awareness regarding the currently selected intercept, whereas the right display is located at the Engineering Workstation position and provides awareness of the functionality of the systems under test, as well as the estimated positions of tracked aircraft.

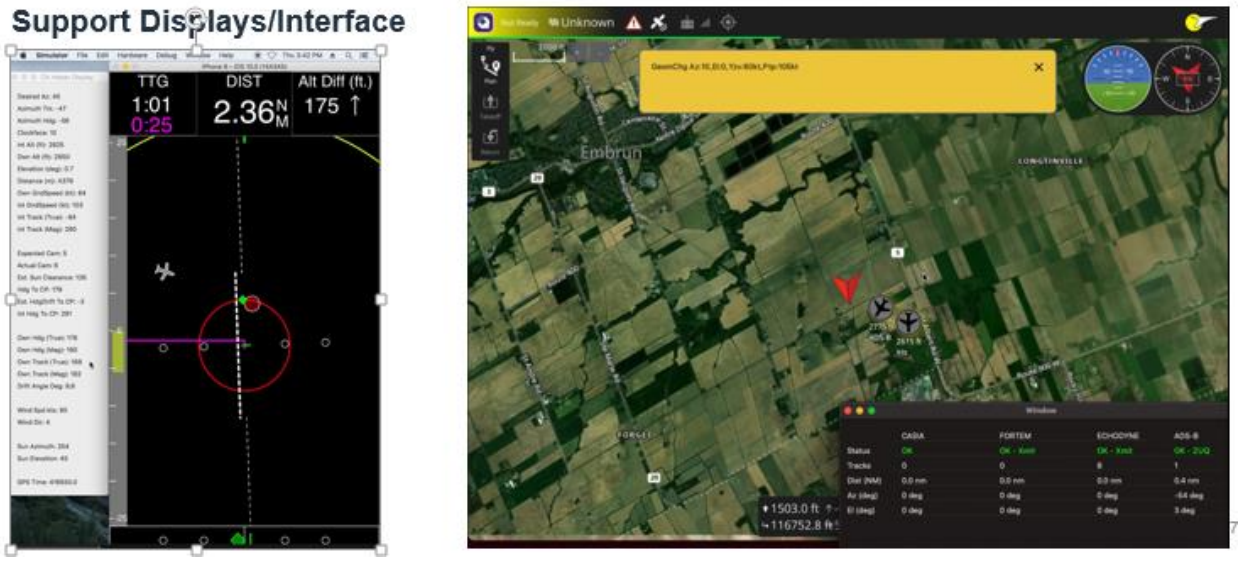

Figure 6: DAA Support Displays (Bell 205)

The Intruder aircraft was equipped with a Seated Rack installation as shown in Figure 4. The seated rack installation provided the ADS-B functionality for the Intruder aircraft as well as the interface to the aircraft's Inertial Navigation System, data aggregation and recording, as well as providing the necessary data stream to drive the iCollide display symbology (Figure 7), which was presented to the Intruder pilot via an Apple iPhone mounted in the cockpit. Further detail regarding the iCollide display is given in section 3.5.3.

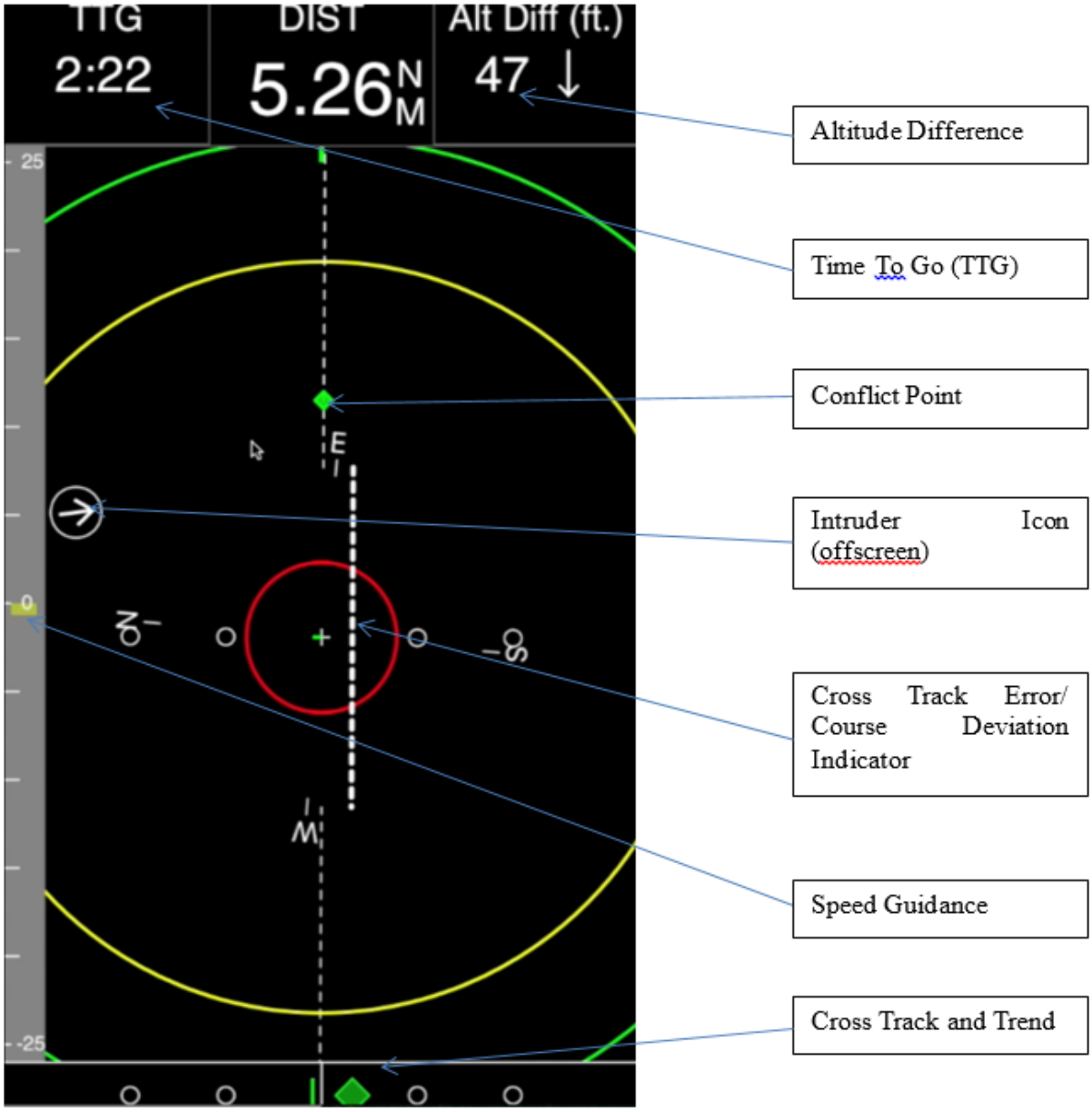

Figure 7: iCollide Guidance

2.1 Radar Authorisation

To perform flight test of the detect and avoid systems, NRC was required by law to obtain a "Radio License" from Innovation, Science and Economic Development Canada. The license was a developmental license that was valid for a full year spanning the flight test period.

3.0 HOST AND INTRUDER AIRCRAFT AND SUPPORTING SYSTEMS

3.1 Host Surrogate RPAS – NRC Bell 205 Airborne Simulator

The aircraft chosen to serve as the surrogate UAS for this investigation was the NRC Bell 205 Airborne Simulator, a single main rotor helicopter that has been extensively modified for fly-by-wire operation (Figure 8).

Figure 8: NRC Bell 205 Airborne Simulator

The FRL has operated variable stability (fly-by-wire) helicopters in airborne simulation and systems development modes for nearly four decades. The Airborne Simulator, based on a Bell 205 A-1 is the third generation of such machine developed at FRL.

The Bell 205 is a commercially popular single-engine utility helicopter. It is powered by a Lycoming T-53-13A turboshaft with a rated take-off output of 1250 shp and has a maximum gross weight of 9500 lb. The Airborne Simulator's design philosophy attempts to be non-invasive to the original systems, making the FBW systems passive "cargo" to the extent possible. Fuel system, electrical system, flight control hydraulics, airframe, drivetrain and powerplant remain essentially unmodified.

A number of modifications were incorporated into the Bell 205 for service as an Airborne Simulator. The rotor stabilizer bar has been removed, sacrificing a degree of stability for enhanced control effectiveness. A flapping angle transducer has been mounted in the rotor head. Internally, the cockpit has been modified to situate the command/Safety pilot on the left side. The right cockpit station has been modified with project displays, a force-feel system and/or electronic inceptors to accommodate the evaluation pilot. In the cabin, an optional engineering workstation was available to monitor project systems.

Once the safety pilot engaged the fly-by-wire system via a pushbutton on the cyclic grip, control of the aircraft was transferred to the autopilot flight control laws. The control laws were configured as:

Pitch Axis: Speed control,
Roll Axis: Track over ground control,
Yaw Axis: Turn coordination,
Heave Axis: Altitude hold

The Flight Control Computer (FCC) contained the control laws and augmentation required to perform the experiments at hand. Supporting the FCC was a Health Monitoring Unit (HMU), which performed safety checks on the FBW system to ensure correct operation. The FCC generated actuator commands, which were then processed by HMU and discrete logic circuits that were capable of disengaging the FBW in the event of an actual or predicted fault condition. The safety pilot was capable of manually disengaging the FBW system at any time in two ways: through selected disengagement via switches (the nominal method for disengagement), and by manually overriding the controls. Since the safety pilot's controls were mechanically connected to the aircraft actuators via the standard set of push rods and linkages, and the safety pilot always remained 'hands-on' the controls they were always aware of how the experimental FBW system was performing and were able to disengage at a moment's notice.

The design of the NRC Airborne Simulator provided for flexibility in the integration of control software and test hardware. In the case of the Bell 205, the benign handling qualities of the host vehicle allowed the safety pilot to assume virtually complete responsibility for flight envelope protection and reversionary control. Built-in diagnostics supplemented the safety pilot by monitoring the integrity of the sensor data and the command path signal. The flexibility inherent in this architecture allowed experimental software to be coded and flown with minimal overhead for validation and testing. When used as an in-flight simulator, the NRC Bell 205 offered an essentially perfect "visual system" (a.k.a. the view of the outside world through the cockpit windows) and "motion system" (real flight accelerations). A programmable digital force-feel system and configurable displays completed the ability to configure the airborne simulators for a broad range of flight tests in short order.

Figure 9 presents a block diagram of the equipment on the Bell 205 that was installed to support the investigation of the DAA sensors under test. The primary means of data distribution on the NRC Bell 205 Airborne Simulator was via Ethernet packets. Reference 6 contains a detailed listing of the network architecture and packet formats for the standard 'project' system installed on the aircraft. Data packets from the aircraft network were received by the Apple Mac-Mini™ computer installed in the Engineering workstation which was configured to run the display packet generation software.

The engineering workstation computer also communicated directly with the GDL-90 ADS-B transceiver via an ARINC 429-to-Ethernet converter. This allowed for the host Bell 205 to use its high resolution INS (Reference 7) as a substitute for the ADS-B position/velocity/altitude source. It further facilitated the transmission of the conflict point to coordinate the intercepts. Traffic report data from the ADS-B unit was received via a RS-422 - to - Ethernet conversion, and employed the GDL-90 message format as specified in Reference 8.

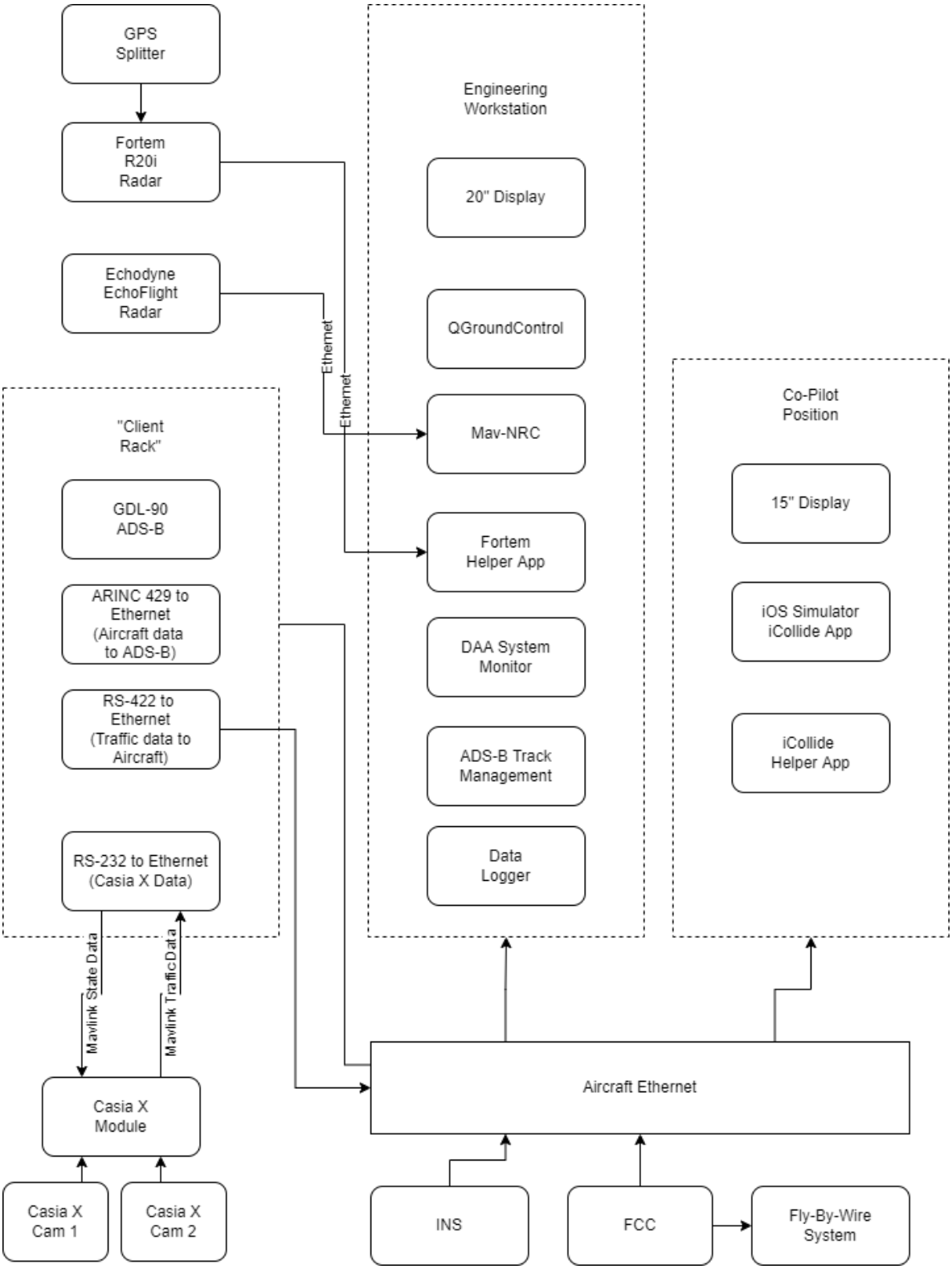

Figure 9: NRC Bell 205 DAA System Block Diagram

3.2 Intruder Aircraft – Seated Rack

To allow for a rapid instrumentation, and flexible choice of intruder aircraft it was decided to mount the hardware in an enclosure that was designed to be installed in an aircraft seat and fastened via seat belts. Figure 10 presents a photograph of this "seated rack", and two cutaway drawings showing the various components.

Figure 11 shows a block diagram of the equipment setup. Unlike the installation in the host surrogate UAS, the intruder GDL-90 ADS-B transceiver was not connected to the aircraft INS via an ARINC to Ethernet converter, and instead relied on the GDL-90 internal GPS receiver to provide a position solution. A GPS splitter was required to provide the GPS receiver in the GDL-90 with connection to a suitable GPS antenna. For all intruders used in this project, the GDL-90 in the seated man rack was connected to the 'project' GPS antenna which was a separate antenna that was connected to the NRC developed INS; as opposed to the GPS antenna used for avionics/navigation systems installed in the cockpit.

The most common method of installing a Garmin GDL-90 ADS-B transceiver in an aircraft would involve connecting its RS-422 (differential serial) output to a display such as the Garmin GMX-200. For the purposes of this project, however, it was desired to employ a proprietary display intended specifically for collision avoidance flight test. This necessitated decoding, and conversion of the GDL-90's RS-422 data stream.

The GDL-90 was connected to the Mac-mini data aggregator via a pair of serial to Ethernet converters. The RS-232 to Ethernet converter was connected to the altitude port of the GD-90; whereas the RS-422 to Ethernet converter was connected to the Traffic Data port. To employ the GDL-90 system it was also necessary to provide it altitude information externally via serial (RS-232).

The Mac-mini was configured to automatically power-up and restore running programs after power interruption. This allowed for the system to be started by simply applying project 28VDC power. Additionally, the computer was configured to "share Ethernet"; thereby allowing the built-in Wi-Fi to serve as an access point to the aircraft's network. This Wi-Fi access point was then used to connect to the display iPhone that ran the intruder iCollide software to provide the guidance for conducting intercepts.

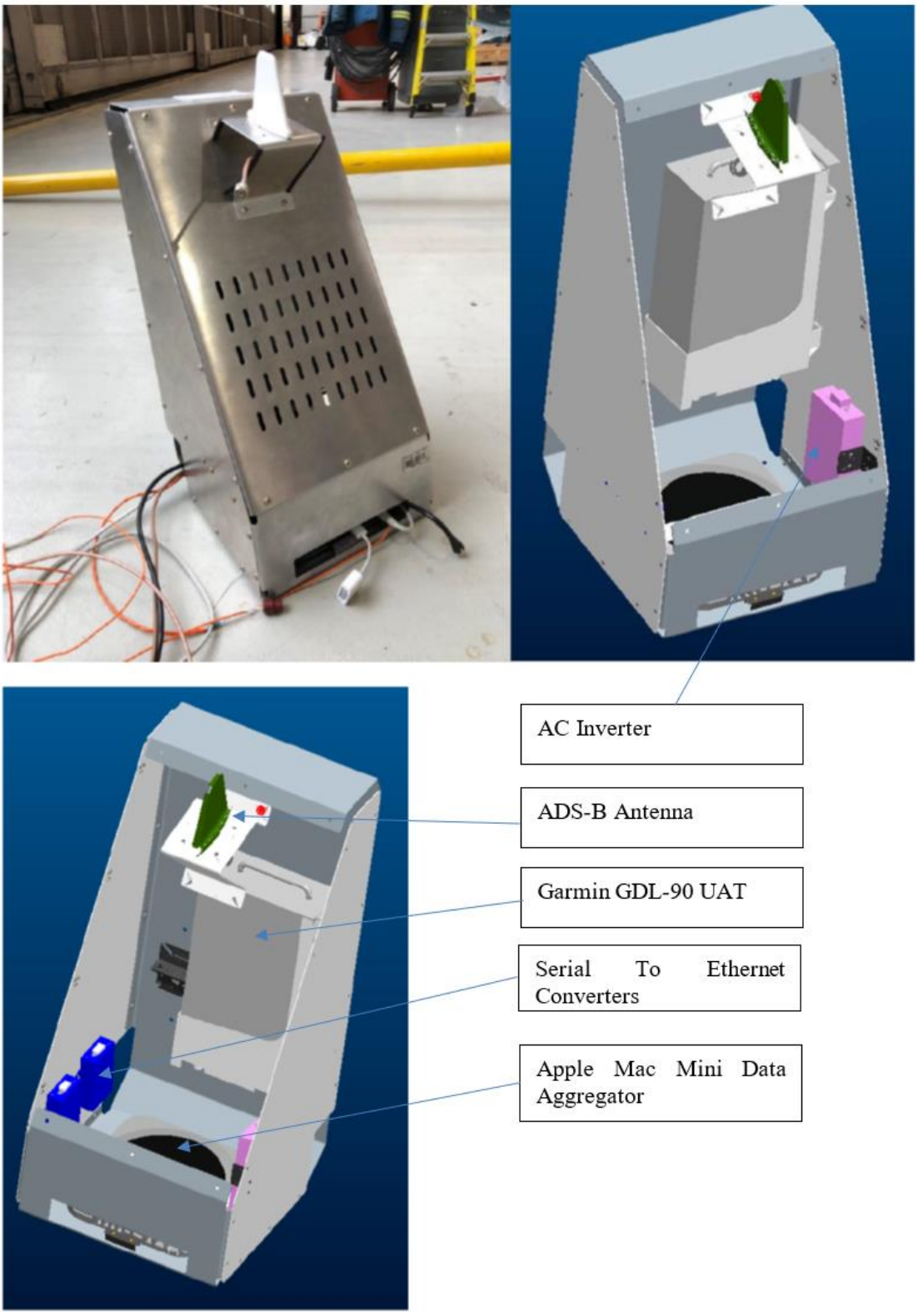

Figure 10: Seated rack hardware installation

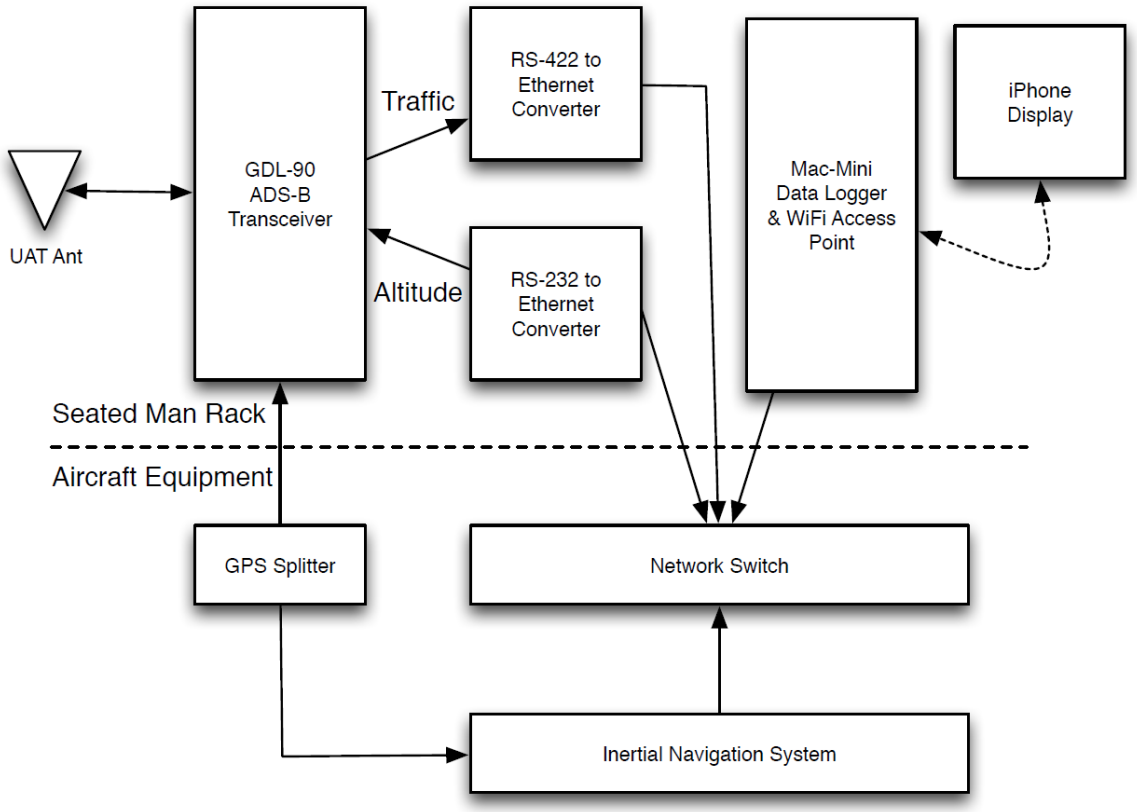

Figure 11: Seated rack block diagram

3.3 Bell 206 Jetranger

The Bell 206 Jetranger (Figure 12) is a two bladed single engine light helicopter with a maximum gross weight of 3,200 lb. The NRC Jetranger has been equipped with a comprehensive PC/104 based instrumentation suite including a high accuracy INS. The aircraft is routinely used as a training platform for NRC's two medium experimental fly-by-wire helicopters, and also has been equipped to perform human factors evaluations regarding night vision goggles. The main rotor diameter is 33 feet and the cruise speed for the Bell 206 Jetranger is 86 knots.

The Jetranger was selected as an intruder for this project as it is believed to be representative of the small helicopter traffic that RPAS may encounter at low altitudes. The Jetranger was used for both cruise flight intercepts, where the intercepts were conducted at a ground speed of 80 mph, and intercepts where the host Bell 205 was in a hover.

Figure 12: NRC Bell 206 Jetranger

3.4 Harvard Mk IV (CF-PTP)

The NRC Harvard Mark IV (T-6) research aircraft (Figure 13) was initially selected as the 'intruder' aircraft for this project. It was selected for this role as it was the aircraft within NRC's fleet that was most representative of the size and speed of typical General Aviation traffic. As well, it contained a high accuracy INS to serve as truth data for Time and Space Position Information (TSPI).

The Harvard is a two-crew tandem configuration, with the rear cockpit serving as the dedicated research station. The aircraft has a 42 ft wingspan, and cruises at approximately 120 knots airspeed. By comparison, a Cessna 172, the most popular light aircraft, has a 36 ft wingspan and also cruises at 120 knots. Intercepts using the Harvard were conducted at approximately 110 knots groundspeed.

The seated rack was installed in the rear cockpit. The iPhone display was mounted in a modified phone case that was attached to a bracket on the left side of the front cockpit instrument glare shield.

Figure 13: NRC Harvard Mk IV

3.5 iCollide Display

The National Research Council of Canada (NRC) has been conducting research into DAA technology since 2009 and is actively collaborating with civil aviation regulators and standards bodies regarding the evaluation of candidate DAA technologies. These efforts have emphasized the need for improved methods and techniques to flight-test a DAA system. The stepped approach supported by regulatory authorities and standards bodies consisted of

1) sensor data collection;
2) system evaluation via simulation; and ultimately,
3) demonstration via flight test.

To support flight test, there is a need to define and develop thorough in-flight validation techniques that permit the conduct of near-miss approaches between two aircraft at variable intercept azimuths and elevations. Only then can one examine, quantify and prove the ability to detect and avoid other traffic.

In most cases, having two aircraft arrive at a predetermined position at a chosen time, while maintaining a constant geometry, requires the solving of two simultaneous four-dimensional (longitude, latitude, altitude, and time) navigation problems. Those encounter trajectories must be simultaneously followed by both aircraft prior to the initiation of the collision avoidance maneuver. Allegorically speaking, one must solve the “detect and collide” problem to enable investigation of the “detect and avoid” problem.

The classical technique for conducting near-miss intercepts employs the initial point (IP) set up, which involves two aircraft departing initial points simultaneously at predefined velocities and track angles to arrive at the same location.

The drawbacks of the classical IP technique are:

1. It requires rigid planning that is not easily adapted to changes in airspace access, winds, weather etc.
2. It is inefficient for small RPASs with limited endurance, and unnecessarily expends valuable flight test time by requiring transits to pre-planned IPs.
3. It is not accurate, since displays intended for en-route navigation of aircraft were not designed to provide course and speed guidance of sufficient precision to conduct intercepts with other aircraft.
4. There is often no direct feedback or guidance of cross track and/or speed error provided to the pilot; typically, pilots fly fixed track angle, heading and speed, which can result in an integrated error.

NRC has been conducting DAA near miss flight testing since 2009. Two approaches for conducting collision intercepts have been developed over this time; both involving the use of display guidance supplied via a smartphone application (i.e. iCollide) to the pilots to assist in the conduct of the maneuvers. For this trial, iCollide V2, as detailed in Reference 9 was employed. A brief overview of the application/approach is provided below.

The approach for iCollide V2 involves the calculation of a conflict point, and an arrival time for both aircraft as well as the provision of lateral and speed guidance.

3.5.1 Collision Geometry

Collision intercepts are a four-dimensional problem; at least two aircraft must intersect in both space and time. The intersection converges into a collision course when both aircraft approach a point sufficiently close in space to penetrate the collision volume at time t=0. Figure 14 presents a generalised and simplified collision course geometry in 3D, with the intruder aircraft represented by the point I and the unmanned aircraft represented by the point O (ownship). Note that winds are not considered in this analysis. Collision timings and speeds are calculated based on ground speed.

The ownship and intruder velocity vectors are indicated by V_O and V_I respectively, while κ and η indicate azimuth and elevation angles in the host reference frame. Both vectors may be multiplied by a time offset t, defined as seconds until impact, to compute the distance. This distance may be updated at each time step, the interval for which is defined by the sensor scan rate or the avoid algorithm update rate. The angles α and γ are of principal interest and can be derived from the cosine law side-angle-angle formulas.

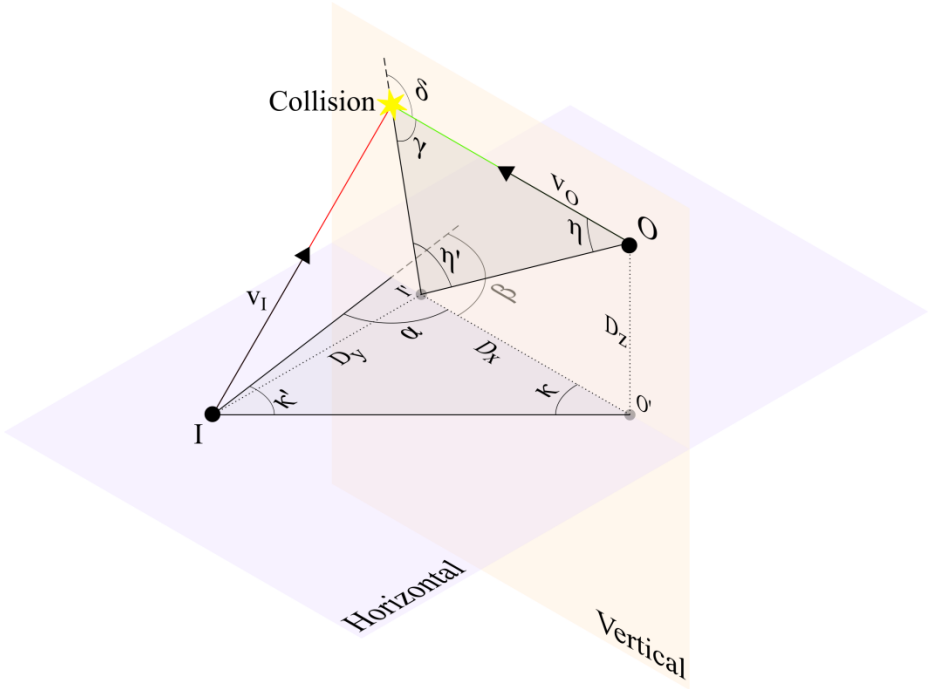

Figure 14: Collision geometry - Quantification of relevant parameters

3.5.2 Determining the Location of the Conflict Point

The conflict point is represented by the intersection of the ownship and intruder velocity vectors. Its location may be determined in world-referenced coordinates (e.g. UTM) provided the initial positions of the ownship and intruder, and desired azimuth κ' are known as follows:

$$TrackCP_o = atan2(E_i - E_o, N_i - N_o) + \kappa'$$

Where:

$TrackCP_o$	is the required track angle to the conflict point for the ownship relative to true north
E_i	is the easting of the intruder in UTM coordinates
E_o	is the easting of the ownship in UTM coordinates
N_i	is the northing of the intruder in UTM coordinates
N_o	is the northing of the ownship in UTM coordinates
κ'	is the desired collision intercept azimuth
atan2	is a four quadrant arc tangent function

Once the angle α has been solved (in degrees), κ may be easily determined by:

$$\kappa = 180 - \alpha - \kappa'$$

Once a collision intercept run has started the location of the conflict point must be held fixed and used as input to the guidance provided by the 4D navigation display. Upon start of the intercept, the location of the conflict point may be determined by:

$$DistCP_o = \frac{sqrt((N_o - N_i)^2 + (E_o - E_i)^2) * sin(\kappa)}{sin(\alpha)}$$

$$CP_N = N_o + \sin(TrackCP_o) * DistCP_o$$
$$CP_E = E_o + \cos(TrackCP_o) * DistCP_o$$

Where:

$DistCP_o$	is the distance from the ownship to the conflict point in meters
CP_N	is the distance from the UTM northing of the conflict point in meters
CP_E	is the distance from the UTM easting of the conflict point in meters

3.5.3 iCollide – Fine Guidance to Conflict Point

Upon engagement of the fly-by-wire controls in the Bell 205, the fixed location of the conflict point and arrival time were transmitted to the intruder aircraft and the displays automatically transitioned to present fine guidance to the conflict point as shown in the screen capture of Figure 15. The text block in the top right of the display indicated the time remaining prior to the planned arrival at the conflict point (TTG), and was calculated at the time of engagement of the fly-by-wire controls based on distance to the conflict point and the selected groundspeed (nominally 60 knots for the Bell 205 for these flight tests). The rightmost text block displayed the relative altitude between the Surrogate RPAS Bell 205 and the intruder, with the sample screen capture indicating the intruder was 47 feet below the ownship altitude. Once the conflict point was fixed in space, the hollow diamond icon was filled with a solid green colour. The desired track to the conflict point was indicated by the dashed white line. The central section of the display features a course deviation indicator where each white hollow dot represents 500 feet of cross track error, and the thick dashed white line represents the location of the desired ground track (e.g. in Figure 15 the aircraft is left of track and needs to correct by a slight right turn input). A green line drawn from the ownship cross symbol represents the rate of change of the cross track error, with the sample screen capture of Figure 15 indicating that the ownship is drifting left away from the desired ground track.

During this guidance state the display would automatically proceed to a zoom state that ensured the conflict point was visible, in an attempt to reduce potential distraction from the automatic scaling of the range ring symbols. Slight changes to the range ring colour scheme were also made:

a. 1 nautical mile: Red
b. 5 nautical miles: Yellow
c. Required separation distance: Green

For much of the duration of the intercept the intruder icon would have to be drawn off-screen. Rather than simply remove the intruder icon from the display it was decided to draw an arrow symbol on the screen bounds at the relative bearing, with the arrow direction representing the intruder track angle.

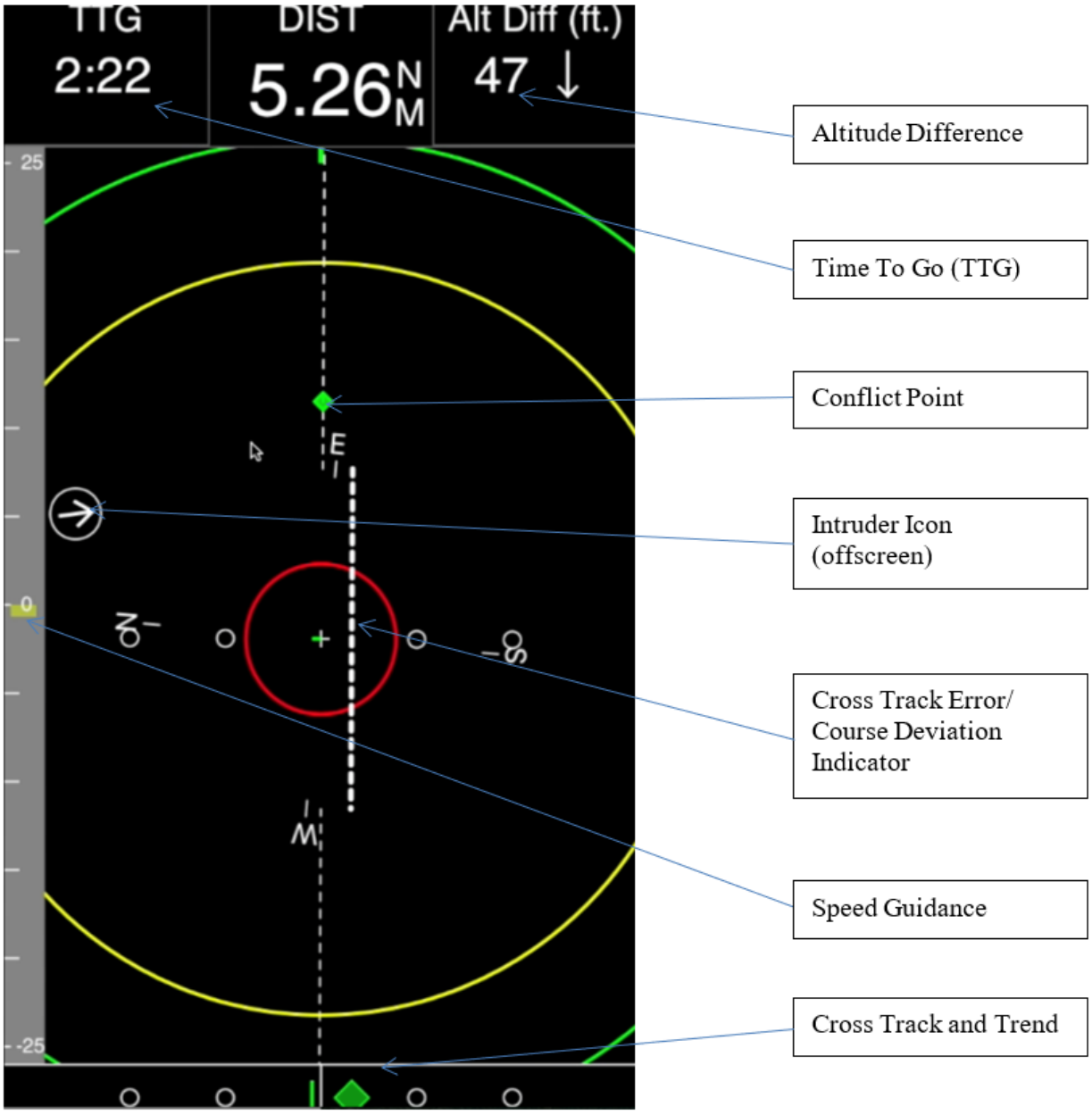

Figure 15: iCollide V2 Fine Guidance to Conflict Point

Speed guidance was provided in the form of a tape on the left hand side of the screen. The nominal required ground speed was determined from the distance to the conflict point divided by the remaining TTG. The current measured ground speed was then subtracted from the nominal required speed and displayed to the pilot as a bar on the tape. The overall scaling was such that 25 knots of ground speed error was full scale. The sense of the bar was such that a positive bar (upwards pointing) required the pilot to increase speed.
The cross track error and rate were re-displayed at the bottom of the screen. The only difference between these symbols and the course deviation indicator was that the coarse deviation symbols rotated with ownship track angle whereas the cross track error and rate symbols remain fixed to the bottom of the screen. In practice the split bar course deviation indicator was a more compelling and useful cue.

3.6 Companion Display (NRC-Bell 205 Co Pilot Station)

A companion display application (Figure 16) was developed to run in a window adjacent to the iOS simulator on the host surrogate RPA.

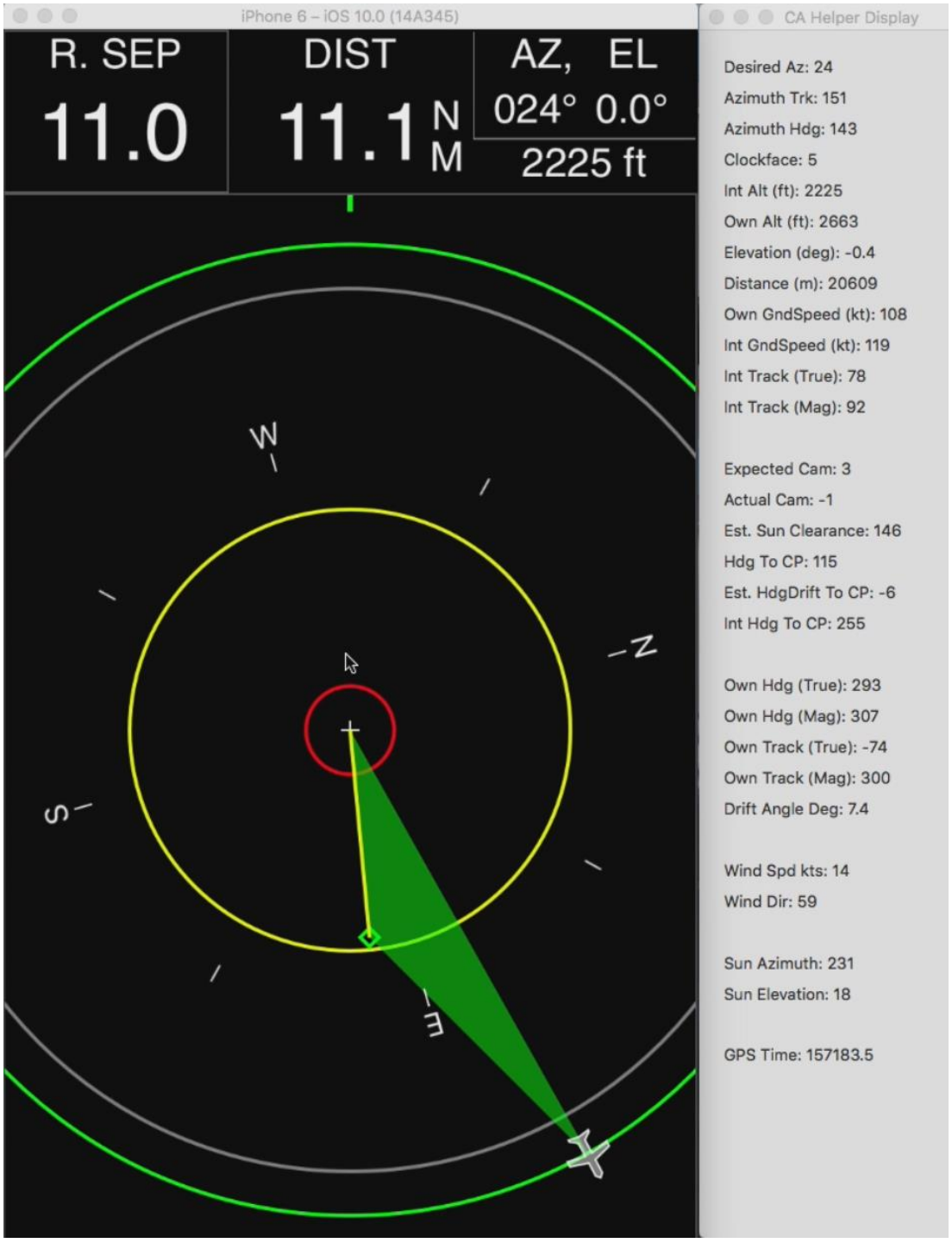

Figure 16: Companion display (right) and iCollide in iOS simulator (left)

The companion display was configured to provide display of key parameters in a tabular/text format. The companion display provided some information that was not provided directly by the iCollide display as described in Table 1.

Table 1: iCollide Helper Application Parameters and Description

Field	Label	Description
1.	Desired Az	Desired Azimuth - This is the user selected collision geometry (also displayed on iCollide)
2.	Azimuth Trk	The current azimuth to the intruder as measured relative to the ownship's current ground track
3.	Azimuth Hdg	The current azimuth to the intruder as measured relative to the ownship's current heading
4.	Clockface	The current azimuth to the intruder as measured relative to heading, but converted into a 'clockface' representation for consistency with normal cockpit protocols for identifying traffic (e.g. "traffic 2 o'clock low, 3 miles")
5.	Int Alt	The intruder aircraft's GPS altitude in feet
6.	Own Alt	The ownship GPS altitude in feet
7.	Elevation	The elevation angle from the ownship to the intruder (in degrees)
8.	Distance	The separation distance from the ownship to the intruder (in meters)
9.	Own GndSpeed	The groundspeed of the ownship (in knots)
10.	Int GndSpeed	The groundspeed of the intruder (in knots)
11.	Int Track True	The track angle of the intruder relative to true north (in degrees)
12.	Int Track Mag	The track angle of the intruder relative to magnetic north (in degrees)
13.	Expected Cam	The camera in the PICAS array that the intruder is expected to be visible in
14.	Actual Cam	The camera in the PICAS array that the intruder is currently visible in (-1 implies the intruder is outside the field of view)
15.	Est Sun Clearance	The angle between the expected camera with the ownship pointing along the ground track to the CP and the solar azimuth (sun angle)
16.	Est Hdg Drift To CP	The estimated delta between heading and track when proceeding along the ground track to the CP
17.	Own Hdg True	The ownship heading relative to true north
18.	Own Hdg Mag	The ownship heading relative to magnetic north
19.	Drift Angle	The current delta between ownship track and heading
20.	Wind Spd	The estimated wind speed (in knots)
21.	Wind Dir	The estimated wind direction (in degrees)
22.	Sun Azimuth	The estimated azimuth of the sun (in degrees)
23.	Sun Elevation	The estimated elevation of the sun (in degrees)
24.	GPS Time	GPS Time in seconds (used for synchronizing video to data)

The data to be displayed by the companion display was transmitted by the data aggregator computer via a UDP packet on port 8552.

4.0 TEST OBJECTIVES AND PLANNING

The flight testing was planned into 3 phases:

Phase 1 – Airworthiness test of externally mounted equipment.
Verify physical integrity of sensor installation through the main Bell 205 flight envelope (Hover to Vne KIAS) and up to 2g. Test technique included a speed sweep (including dwells at low speed and high speed), wind up turns, max climb and autorotation.

Phase 2 – Sensor tests at lower speeds using Bell 206 helicopter intruder as a target.
The flight test techniques in this phase consisted of pointing the sensors at the intruder aircraft and determining the range and accuracy of the sensor given a variety of host and intruder trajectories and sensor backdrops. The NRC Bell 206 was to be the intruder aircraft. General vehicle speeds were 0 knots (i.e., hover) or 60 knots for the NRC Bell 205 and 60 mph[1] for the NRC Bell 206. These tests were intended to be representative of a hovering RPAS encountering low level traffic.

The test technique involved a careful selection of planned collision trajectories including:

1. Enroute formation flying;
2. Low altitude (from ground to 100' above ground level) collision trajectories;
3. Higher altitude collision trajectories (nominally 2500') with the intruder both above and below the horizon;
4. Circuits to a stationary host.

Phase 3 – Sensor tests at higher speeds and altitudes using fixed wing intruder aircraft as a target.

The flight test techniques consisted of pointing the sensors at the intruder aircraft and determining the range and accuracy of the sensor given a variety of host and intruder trajectories and sensor backdrops. The NRC Harvard was the intruder aircraft. General vehicle speeds were 60 knots for the NRC Bell 205 and 105 knots for the NRC Harvard. The test technique involved a careful selection of planned collision trajectories including:

1. Higher altitude collision trajectories (nominally 2500' AGL) with the intruder both above and below the horizon;
2. Higher altitude (2500' AGL) deliberate miss trajectories based on speed and/or lateral offset;
3. Pure pursuit task collision trajectories.

In practice, after the Phase 1 testing, the use of the helicopter and fixed wing intruder aircraft was mixed without the clean separation into phases. This was partly due to the availability, service history and test range availability. Flight tests at altitude were conducted away from the Ottawa International Airport (ICAO identifier CYOW) in a controlled block of airspace to minimise potential conflicts with other air traffic including general aviation traffic. These flight test areas included the airspace bounded by the area of authorisation for the radars (a 37 km circle centered on the village of Casselman at an altitude of 10000' MSL and below) - See Figure 17. Low altitude testing and circuit testing was conducted at the Pendleton, Ontario Airport (ICAO identifier CNF3). The weather limits included a minimum in-flight visibility of 10 nautical miles and a lowest ceiling of 2,000' above the test altitude. These testing limits were used to ensure

[1] Speeds for the Bell 206 are listed as miles per hour as opposed to knots since this is what is displayed on the airspeed indicator

good visual conditions for the aircraft pilots to acquire visual contact and maintain visual separation. The testing wind limit was 25 kts.

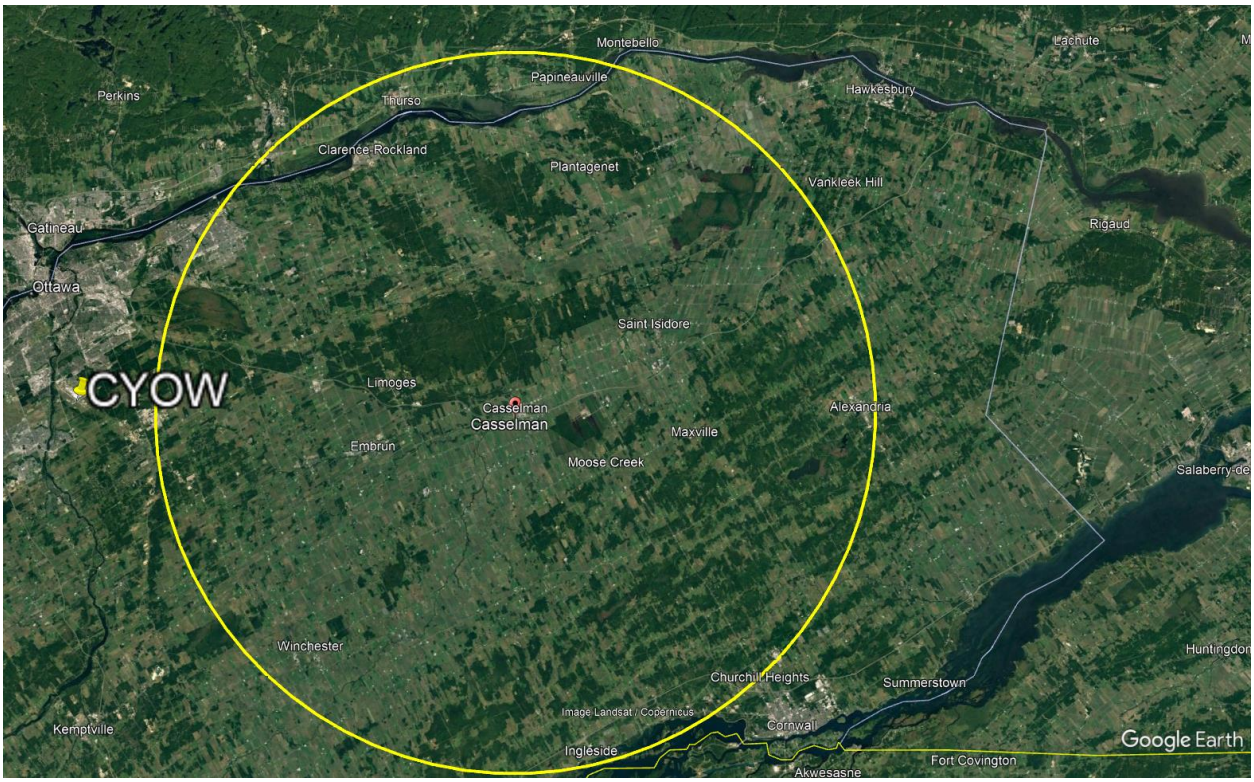

Figure 17. Authorised RADAR Test Area

4.1 Test Techniques

The following paragraphs include a description of the test maneuvers that were planned.

4.1.1 Enroute formation flying:

This test maneuver provided an initial look at radar and optical tracking in a benign environment. The test aircraft (host and intruder) joined and departed the airport in line astern position, with the Intruder in the lead. The host aircraft coordinated the test point and both aircraft varied their speed to expedite lateral separation (5 km or 2.5 nm) separation to be achieved if possible, and then reduce separation back to a loose formation position. Distance was determined by reference to the digital readout on the iCollide guidance as well as visual estimation. The pilot in the intruder aircraft was responsible for coordination with ATC as formation lead, and the pilot of the host served as the test director between the aircraft.

When possible, on the RTB leg, the aircraft would form a loose formation and the sensors on the host would track the intruder.

4.1.2 Low altitude (Host at ground level to 100’ AGL) collision trajectories:

The host aircraft started in a hover at suitable location that permitted the intruder aircraft sufficient space to approach. Hover heights were specified in the test matrix. The intruder aircraft approached from different azimuths at an airspeed of 60 mph. Both aircraft maintained the same height above ground with the Intruder commencing overshoot/recovery prior to 200’ lateral distance from the host.

4.1.3 Low altitude offset trajectories:

The host aircraft started in a hover at a location at a suitable location that permitted the intruder aircraft sufficient space to approach. Hover heights for the host were specified in the test matrix. The intruder aircraft approached from different azimuths at an airspeed of 60 mph. Both aircraft maintained the same height above ground with the Intruder commencing overshoot/recovery prior to 200' lateral distance from the host.

The intruder pilot visually adopted an intentional miss trajectory over the ground with an offset of 1000 feet from the host.

4.1.4 Higher altitude collision trajectories (2500' AGL):

When instructed by the host aircraft pilot after the required initial separation distance had been achieved, the intruder aircraft turned and followed the iCollide guidance. The intruder pilot maintained airspeed, as indicated in the test matrix and iCollide guidance, to achieve the conflict point at the desired time. The intruder aircraft overflew/underflew the host aircraft, marking the completion of the test point.

4.1.5 Higher altitude - deliberate miss trajectories based on speed:

When instructed by the host aircraft pilot, after the required initial separation distance had been achieved, the intruder aircraft turned and followed the iCollide lateral guidance, however maintained a higher airspeed (Nominally $\Delta 1 = 5$ kts and $\Delta 2 = 10$ kts) than the guidance displayed. Airspeed was indicated in the test matrix. For high azimuth conditions this resulted in the intruder aircraft missing by passing in front of the host aircraft (at a different altitude), which also marked the completion of test point.

4.1.6 Higher altitude - deliberate miss trajectories based on lateral offset:

When instructed by the host aircraft pilot, after the required initial separation distance had been achieved, the intruder aircraft turned and such that the guidance displayed one dot right of desired track for head-on (0°) and 10° cases and one dot left for -45° (as detailed in the test matrix). The intruder maintained airspeed, as indicated in the test matrix and iCollide guidance. This resulted in the intruder aircraft missing by passing in front of the host aircraft (at a different altitude), which also marked the completion of test point

4.1.7 Circuits to a stationary host:

The host aircraft started in a hover at a location at a suitable location that permitted the intruder aircraft sufficient space to approach. Hover heights were specified in the test matrix. The intruder aircraft approached on different azimuths at an airspeed of 60 mph. Altitude varied from a descent from a 500' circuit height to ground level with the Intruder coming to the hover 200' horizontally and 10' above the host on an approximate 3 degree glide path.

5.0 SYSTEM INTEGRATION

This section describes the physical and data integration aspects of each of the DAA sensors under test.

5.1 Iris Automation Casia X

5.1.1 Physical Installation

The Casia X system can be configured with up to 5 cameras for a full 360-degree horizontal field of view coverage. For the purposes of this flight test a 2-camera arrangement was used, covering a total field of view of 144 degrees. All intercepts were planned for the intruder to be within the field of view of all systems under test (note that the radar systems each had a 120-degree horizontal field of view).

The cameras were installed within fairings on the FLIR mount arm located on the left side of the aircraft as shown in Figure 18. The fairings included threaded mounts for neutral density 'haze filters' that protected the camera lens from dirt and debris and ensured that the installation was sealed to prevent potential foreign object debris (e.g. components of the camera assembly coming loose owing to aircraft vibrations). An inspection window was located on the side of the fairings to allow for the focus ring of the cameras to be verified. The cameras were focused by Iris Automation prior to receipt, and were marked with 'anti-tamper' paint.

The cameras were connected to the Casia X module which was installed on a panel on the rear of the Engineering Workstation rack within the cabin of the Bell 205 as shown in Figure 19. The camera installation required a calibration step to correlate the image plane to the aircraft (extrinsic calibration). During this step it was observed that the Casia module did not allow for the cameras to be installed in an inverted orientation, thus the installation was modified to orient the cameras 'right side up'.

Figure 18: Casia X Camera Installation

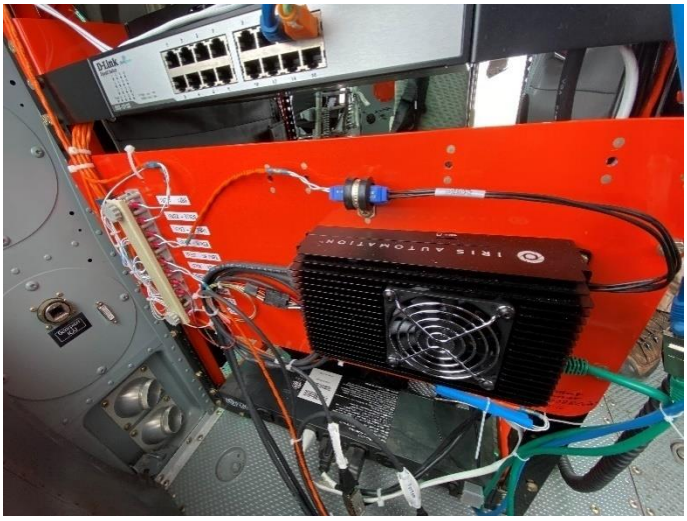

Figure 19: Casia X Module Installation

5.1.2 Data Interface

The Casia X module is intended to connect to an on-board autopilot via the Mavlink data protocol. The Casia system relies upon aircraft state information (position, and attitude) as provided via Mavlink to estimate the position of intruder aircraft it detects. The state data was sent at a rate of 15 Hz. The Casia module is capable of issuing automatic avoidance commands via Mavlink to a coupled autopilot, however this functionality was not used for these flight tests.

The Casia module was interfaced to the NRC Bell 205 via the in-house developed 'MavNRC' application, which acts as communications bridge between the proprietary data format employed on the aircraft, and the open Mavlink standard. This enabled rapid integration of the Casia system including the ability to record Casia generated traffic messages along with the standard suite of recorded data, in the FRL data format.

Casia X signals the presence of proximate traffic through the Mavlink ADSB_VEHICLE message (#246) which contains the following fields:

Field Name	Type	Units	Values	Description
ICAO_address	uint32_t			ICAO address
lat	int32_t	degE7		Latitude
lon	int32_t	degE7		Longitude
altitude_type	uint8_t		ADSB_ALTITUDE_TYPE	ADSB altitude type.
altitude	int32_t	mm		Altitude(ASL)

Field Name	Type	Units	Values	Description
heading	uint16_t	cdeg		Course over ground
hor_velocity	uint16_t	cm/s		The horizontal velocity
ver_velocity	int16_t	cm/s		The vertical velocity. Positive is up
callsign	char[9]			The callsign, 8+null
emitter_type	uint8_t		ADSB_EMITTER_TYPE	ADSB emitter type.
tslc	uint8_t	s		Time since last communication in seconds
flags	uint16_t		ADSB_FLAGS	Bitmap to indicate various statuses including valid data fields
squawk	uint16_t			Squawk code

The messages were received by the MavNRC application, and timestamped upon arrival, and additionally re-broadcast to the QGroundControl (QGC) application that was also running on the Engineering Workstation. This allowed for the Casia X detected intruders to be displayed on the QGC moving map. The data received from the GDL-90 ADS-B transceiver was also relayed to QGC for display via the ADSB_VEHICLE message, allowing for improved situational awareness regarding the intruder location, as shown in Figure 20.

The integration was relatively straightforward, once the correct Mavlink version serialization format was sent; however the integration process could be improved through the use of Iris Automation's included 'FlightDeck' web interface. As tested, the only way to know if the system integration was correct was to monitor the Mavlink messages being received from the Casia module. If the integration was incomplete the Casia module would not issue heartbeats, however would issue a STATUSTEXT message indicating that the Casia software was operational. It is recommended that the FlightDeck application also be configured as a supplemental means to indicate meaningful integration and debugging information (e.g. "No heartbeats received", or "Not receiving attitude messages").

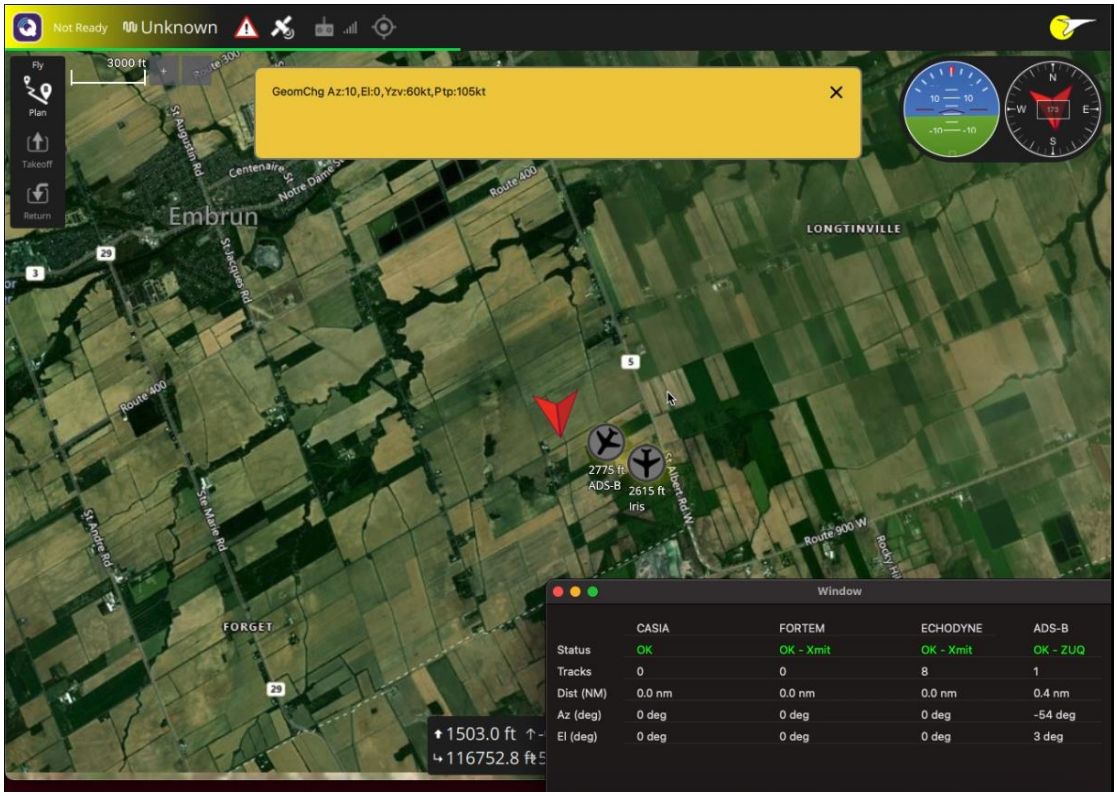

Figure 20: QGroundControl and DAA Helper Application

5.2 Echodyne EchoFlight

5.2.1 Physical Installation

The Echodyne EchoFlight radar was mounted to a generic mount installed on the nose of the NRC Bell 205 as shown in Figure 21. The mount was biased 40 degrees to the port side allowing for the 120 degree Field of View of the radar to cover collision azimuths between +20 to -100 degrees as opposed to ±60. This was done under the assumption that the DAA sensor performance would be identical on the left and right side of the aircraft, and that it would be of greater interest to have the ability to test higher azimuths where the visible cross section, and radar cross section of the intruder aircraft would be different.

Power to the EchoFlight unit was routed through a switch box located at the Engineering Workstation location allowing the radar to be rapidly powered down mid-flight.

Control of the radar transmit function was enabled via software communication with the radar over a dedicated Ethernet connection in response to pilot activation of a switch located on the center console of the NRC Bell 205.

5.2.2 Data Interface

The Echodyne EchoFlight radar was configured to transmit TCP packets over its Ethernet interface. A custom integration was performed within the MavNRC application. This integration was responsible for:

1. Establishing the connection to the EchoFlight radar
2. Sending configuration change request messages

3. Receipt of radar Track data
4. Recording and timestamping of radar track data and radar configuration

These functions are further detailed below.

Figure 21: Echodyne (lower) and Fortem (upper) Physical Installation

Establishing connection to the EchoFlight radar: This function ran in a loop that constantly checked to see if a valid Ethernet socket connection to the EchoFlight had been established, and attempted to open a new connection every 5 seconds if no valid connection was detected. This allowed for the integration to be robust to accidental disconnection of the Ethernet, or power interruption to the EchoFlight radar.

Sending configuration change request messages: The EchoFlight radar can be configured with a wide range of variable parameters such as field-of-view, range, tracker settings, transmitter control, etc. These configuration changes were all performed using a dedicated configuration port. During the early stages of the testing the system responses to the configuration messages were simply printed to the terminal window, however in later stages the responses were logged to disk to ensure that the configuration of the radar was logged and recallable.

Receipt of radar track data: Through the configuration port it was possible to configure the radar to transmit raw detection data or tracks. It was decided to only log track data as this resulted in the least amount of data storage/bandwidth, post flight analysis, and likely reflected the most typical application in a third-party integration into an RPA for detect and avoid purposes. As the EchoFlight does not feature an internal navigation solution it transmits track data in local coordinates, requiring the integrator to perform any desired geo-referencing of the track data.

Recording and timestamping of radar data and radar configuration: Radar track data was timestamped with GPS time on decoded receipt, and logged to an FRL format file. During later stages of flight testing the radar configuration responses were logged to disk in a time stamped text file.

Software integration of the Echodyne EchoFlight was well described by the user manual, however since TCP packets were used instead of UDP it was necessary to employ a local circular buffering and parsing

strategy as the packet data received when the recv() function returns may not correspond exactly to a single track data message packet.

5.3 Fortem R20i

5.3.1 Physical Installation

The Fortem R20i was mounted to a generic mount installed on the nose of the NRC Bell 205 as shown in Figure 21. The mount was biased 40 degrees to the port side allowing for the 120 degree Field of View of the radar to cover collision azimuths between +20 to -100 degrees as opposed to ±60. This was done under the assumption that the DAA sensor performance would be identical on the left and right side of the aircraft, and that it would be of greater interest to have the ability to test higher azimuths where the visible cross section, and radar cross section of the intruder aircraft would be different.

Power to the R20i unit was routed through a switch box located at the Engineering Workstation location allowing the radar to be rapidly powered down mid-flight.

Control of the radar transmit function was enabled via software communication with the radar over a dedicated Ethernet connection in response to pilot activation of a switch located on the center console of the NRC Bell 205.

The Fortem R20i features an internal inertial navigation system for georeferencing of track data, and was supplied a GPS antenna connection via a GPS splitter mounted in the cabin of the NRC Bell 205. The GPS antenna was located on the top of the 90 degree gearbox for the tail rotor.

5.3.2 Data Interface

The Fortem R20i was configured to transmit data via a dedicated Ethernet connection using a websocket protocol with JSON data format. The included ICD specified Python 3 as a system requirement, however it is believed that this is only a requirement to use the included sample integration code; browser or server-based integrations using Javascript should be possible. Implementations using other languages (e.g. C/C++) would require the use of libraries.

To simplify the integration process the included sample Python script was used as a starting point for a ‘Helper application’ that ran on the Engineering Workstation and was responsible for:

1. Opening the websocket connection to the Fortem R20i, and subscribing to the track data stream
2. Maintaining an HTTP connection to the Fortem R20i to signal configuration changes (e.g. set radar to transmit, or retrieve status information)
3. Opening a UDP connection to the MavNRC application to receive control requests to set the radar to transmit, or to stop transmitting
4. Opening a UDP connection to the MavNRC application to send decoded track data

These functions are further described below:

Opening the websocket connection to Fortem R20i: Websockets are bidirectional communication protocol that is kept alive until either the client or server terminates the connection. The sample code provided by Fortem was used as a basis for the ‘Helper application’. During the flight test campaign it was noted that the websocket connection would occasionally drop, and never re-establish connection. It is believed that this was caused as a result of a combination of a loose Ethernet cable connection, the high vibratory environment of the Bell 205, and the helper program not having been written to re-try establishing the

connection if it was terminated. This issue was addressed midway through the flight test campaign, resulting in data being acquired for only 45 of the 79 test points conducted.

Maintain HTTP connection to the R20i to signal configuration changes: This function was primarily used to control the transmit status of the radar, as well as to poll for status messages at approximately 0.5 Hz. Selected fields from the status responses were relayed to MavNRC via UDP packet for data recording.

Opening a UDP connection to MavNRC application to receive control requests for radar transmit: The radar transmit function was signaled via a UDP packet from MavNRC based on the status of a center console switch position that was monitored in a shared memory segment and activated by the pilot. On receipt of the control message packet the helper application would issue a websocket request to the R20i to toggle the transmit status of the radar.

Opening a UDP connection to the MavNRC application to send decoded track data: The helper application received JSON encoded messages containing the track data from the R20i. The application would parse the track data and re-package selected data parameters for transmission to the MavNRC application where the packets were time-stamped and recorded to disk for analysis.

The Fortem R20i featured an internal webserver application which proved very useful for changing configuration, and for monitoring the operation of the radar. This tool proved especially useful for verifying the data receipt aspects of the system integration. A sample screen capture from the webserver is shown in Figure 22. Using screen recording of the webserver output allowed for the identification of the dropped connection issue highlighted above, as the webserver continued to indicate tacks and valid status, whereas the Helper application issued no further track updates.

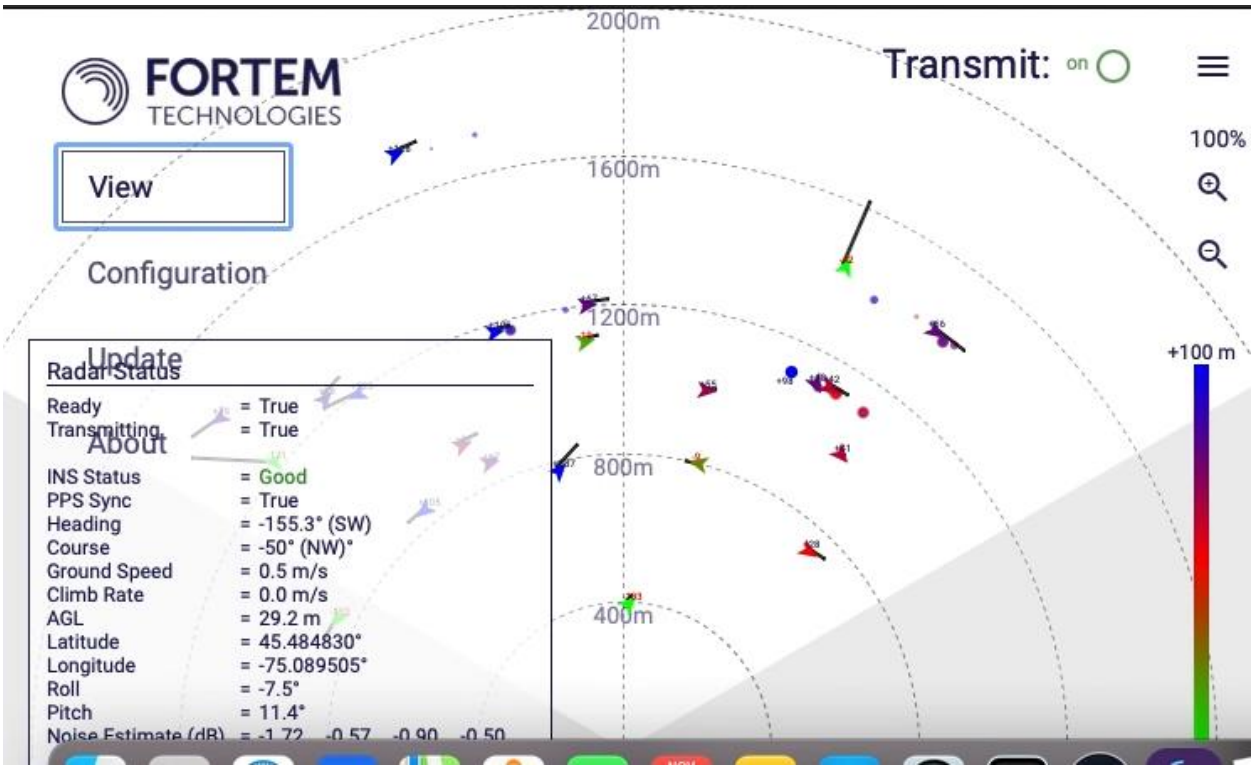

Figure 22: Sample screen capture from the Fortem R20i webserver

5.4 General Observations Regarding System Integration

The task of having to integrate three sensors to a single airborne platform highlighted the fact that there is no common interface standard definition for DAA sensors. Moreover, the three sensors tested required different degrees of integration and levels of familiarity with the basic sensing modality and its associated parameters.

Of the three sensors tested, the Casia X represented the most complete solution as it offered internal threat detection, and included the ability to trigger a pre-programmed avoidance maneuver (e.g. descend and loiter). The avoidance maneuver features of the Casia X were not investigated as part of this project, however. The Casia X also required the least integrator knowledge regarding the sensor itself, and offered no tunable parameters for the camera or detection algorithm (e.g. detection range, sensitivity, etc). An understanding of the importance of extrinsic calibration, was critical, however.

Both the Casia X and the EchoFlight rely upon position and orientation data as supplied from the host aircraft. Orientation errors from low cost/quality gyros as often found on small RPAs may be a cause for concern; as is the potential for calibration error between the host gyro and the camera. A two-degree error, for example, would result in approximately 70 meters of position error for a target at 2km.

The EchoFlight allowed for several sensor parameters to be altered both prior to, and during operation. Determination of the most appropriate values for these parameters required a solid understanding of radar sensing fundamentals as well as concepts related to target tracking.

The R20i featured an internal IMU and GPS receiver; making it unnecessary for the integrator to perform the georeferencing of the radar tracks. In this flight test the GPS signal was supplied from a GPS splitter from the antenna mounted at the top of the vertical tail which was located approximately 10 meters from the radar location. The authors do not recall any means to identify the GPS antenna lever arms to the R20i, and it is suspected that this could have a significant impact on the utility of the georeferenced tack outputs. The R20i did not have as extensive a list of tunable parameters as the EchoFlight, and the included webserver application simplified the process of parameter adjustment and verification.

Both the R20i and the EchoFlight would require intermediate processing for use in DAA applications, as filtering returns from ground obstacles, and identification/prioritization of airborne collision threats is not performed within the radars internal processing. Moreover, none of the tested systems can be considered as ‘plug-and-play’; i.e. one cannot simply connect the output of the sensor to an automatic collision avoidance solution such as ACAS sXu without additional processing.

6.0 FLIGHT TESTS

The airworthiness assessment flight test was conducted on March 9 2022, and consisted of the following test points:

1. Hover
2. Accel to 10 knots groundspeed
3. Accel through translational lift (dwell 30 seconds)
4. Accel in 10 knot intervals 40, 50, 60 knots
5. 2g Wind-up turn at 60 knots IAS
6. Accel 70, 80, 90 knots IAS
7. 90 knot IAS dwell (20 minutes)
8. Max continuous climb at 90 knots (1 minute)
9. 2g Wind-up turn at 90 knots IAS
10. Accel to 100 knots IAS

11. Accel to VNE (109 knots IAS for the current conditions)
12. Autorotation at 60 knots IAS from 3,000 ft

The purpose of the flight was to assess if the installations resulted in any undesirable aircraft vibrations or handling qualities. Throughout the flight no objectionable vibrations or effects on handling qualities were observed by the flight crew. Upon landing the Bell 205 on its mobile platform it was observed that there was only approximately 1 foot of clearance between the lower radar (EchoFlight) and the forward tire of the platform as shown in Figure 23. To mitigate potential safety concerns the radar clearance to the platform tire was a briefing point for each subsequent sortie in this configuration.

Figure 23: Radar clearance with platform tire

Once the airworthiness clearance sortie had been completed, the test campaign advanced to the 'air-to-air' phase. This phase was completed over 8 sorties as described in Table 2. Ninety test points, including 80 intercepts were conducted over 14.7 flight hours. Note that 3 test points were not used as part of the performance analysis as they involved phases of the test where the intruder aircraft was outside of the sensor field of view.

Table 2: Air-To-Air Sortie Description

Sortie	Date	Intruder	# of Test points	Duration (hrs)	Notes
1	May 25, 2022	Bell 206	6	1.4	Transmission of Conflict Point did not work, resulting in a lack of speed guidance, and intercepts being hand flown by both Intruder and Host pilots
2	Aug 5, 2022	Harvard	8	2.0	Transmission of Conflict Point was fixed. Fortem R20 re-configured to 'Airborne' mode. Minor changes to Echoflight software setup (including a typo in the Elevation FOV).
3	Aug 10, 2022	Harvard	11	1.7	EchoFlight elevation mask typo fixed. A loose fastener prevented engagement of the FBW system on the Bell 205.
4	Aug 11, 2022	Harvard	14	2.0	FBW functionality on the Bell 205 was restored.
5	Nov 28, 2022	Bell 206	12 (6 recorded)	1.6	Hovering host sortie. The data recorder 'shutdown' switch was invertedly triggered halfway through the flight.
6	Dec 2, 2022	Bell 206	13	2.0	Hovering host sortie. Fortem helper program re-coded to re-establish websocket connection if dropped.
7	Jan 11, 2023	Bell 206	13	2.0	
8	Jan 16, 2023	Harvard	13	2.0	
		Total	90	14.7	

The 80 intercepts conducted are described in Table 3, including the intercept number, maneuver description, intruder aircraft type, date, and starting altitudes (MSL) for the host and intruder. The approximate ground elevation over the flight area was 200 feet MSL, allowing for an easy approximation to the above ground level.

Table 3: Intercept Description

#	Description	Intruder	Date	Host Altitude (ft MSL)	Intruder Altitude (ft MSL)
1	Level -60 Degrees Azimuth	Heli	May 25, 2022	3,715	3,494
2	Level -20 Degrees Azimuth	Heli	May 25, 2022	3,851	3,564
3	Level -20 Degrees Azimuth	Heli	May 25, 2022	3,730	3,361
4	Level +10 Degrees Azimuth	Heli	May 25, 2022	3,742	3,443
5	Loose formation RTB (Not used for analysis)	Heli	May 25, 2022	3,751	3,518
6	Level -80 Degrees Azimuth	Plane	Aug 5, 2022	2,404	2,474
7	Level -60 Degrees Azimuth	Plane	Aug 5, 2022	2,380	2,450
8	Level -33 Degrees Azimuth	Plane	Aug 5, 2022	2,355	2,501
9	Level -45 Degrees Azimuth	Plane	Aug 5, 2022	2,316	2,567
10	Level -7 Degrees Azimuth	Plane	Aug 5, 2022	2,347	2,571
11	Level +1 Degree Azimuth	Plane	Aug 5, 2022	2,447	2,525

#	Description	Intruder	Date	Host Altitude (ft MSL)	Intruder Altitude (ft MSL)
12	Level -78 Degrees Azimuth	Plane	Aug 10, 2022	5,305	5,311
13	Level -60 Degrees Azimuth	Plane	Aug 10, 2022	5,251	5,360
14	Level -50 Degrees Azimuth	Plane	Aug 10, 2022	5,181	5,311
15	Level -32 Degrees Azimuth	Plane	Aug 10, 2022	5,208	5,311
16	Level -1 Degree Azimuth	Plane	Aug 10, 2022	5,223	5,326
17	Level 0 Degree Azimuth	Plane	Aug 10, 2022	5,199	5,384
18	Level -77 Degrees Azimuth	Plane	Aug 10, 2022	5,223	5,311
19	Level -60 Degrees Azimuth	Plane	Aug 10, 2022	5,193	5,414
20	Intentional Miss -30 Deg	Plane	Aug 10, 2022	5,275	5,523
21	Pursuit -40 Degrees	Plane	Aug 10, 2022	5,317	5,372
22	Level -54 Degrees Azimuth	Plane	Aug 11, 2022	2,607	2,428
23	Level -45 Degrees Azimuth	Plane	Aug 11, 2022	2,450	2,368
24	Level -12 Degrees Azimuth	Plane	Aug 11, 2022	2,589	2,407
25	Level -25 Degrees Azimuth	Plane	Aug 11, 2022	2,571	2,398
26	Level +18 Degrees Azimuth (not used for analysis)	Plane	Aug 11, 2022	2,571	2,398
27	Level -20 Degrees azimuth	Plane	Aug 11, 2022	2,580	2,495
28	Level -100 Degrees Azimuth	Plane	Aug 11, 2022	2,474	2,622
29	Level -55 Degrees Azimuth	Plane	Aug 11, 2022	2,462	2,571
30	Level -1 Degree Azimuth	Plane	Aug 11, 2022	2,422	2,525
31	Intentional Miss -50 Degrees	Plane	Aug 11, 2022	2,453	2,565
32	Intentional Miss -50 Degrees	Plane	Aug 11, 2022	2,483	2,668
33	Level -75 Degrees Azimuth	Plane	Aug 11, 2022	2,483	2,668
34	Level -20 Degrees Azimuth	Plane	Aug 11, 2022	2,465	2,710
35	Level -20 Degrees Azimuth	Plane	Aug 11, 2022	2,474	2,586
36	Low Alt Level Pass -10 Deg	Heli	Nov 28, 2022	321	948
37	Low Alt Level Pass -30 Deg	Heli	Nov 28, 2022	303	948
38	Low Alt Level Pass -45 Deg	Heli	Nov 28, 2022	291	945
39	Low Alt Level Pass -60 Deg	Heli	Nov 28, 2022	306	948
40	Low Alt Level Pass -80 Deg	Heli	Nov 28, 2022	324	1,014
41	3 Deg Glideslope -10 Degrees Azimuth	Heli	Nov 28, 2022	285	972
42	Low Alt Level Pass -10 Deg	Heli	Dec 2, 2022	312	1,169
43	Low Alt Level Pass -30 Deg	Heli	Dec 2, 2022	294	1,154
44	Low Alt Level Pass -45 Deg	Heli	Dec 2, 2022	282	996
45	Low Alt Level Pass -60 Deg	Heli	Dec 2, 2022	300	939

#	Description	Intruder	Date	Host Altitude (ft MSL)	Intruder Altitude (ft MSL)
46	Low Alt Level Pass -80 Deg	Heli	Dec 2, 2022	285	839
47	3 Deg Glideslope -10 Degrees Azimuth	Heli	Dec 2, 2022	306	1,142
48	3 Deg Glideslope -45 Degrees Azimuth	Heli	Dec 2, 2022	291	1,096
49	9 Deg Glideslope -10 Deg Azimuth	Heli	Dec 2, 2022	294	1,208
50	9 Deg Glideslope -45 Deg Azimuth	Heli	Dec 2, 2022	297	1,360
51	Low Alt Level Offset Pass -10 Deg	Heli	Dec 2, 2022	300	999
52	Low Alt Level Offset Pass -45 Deg	Heli	Dec 2, 2022	291	1,129
53	Low Alt Level Offset Pass -60 Deg	Heli	Dec 2, 2022	294	1,075
54	Low Alt Level Offset Pass -80 Deg	Heli	Dec 2, 2022	291	1,105
55	Level -50 Degrees Azimuth	Heli	Jan 11, 2023	2,565	2,428
56	Level -50 Degrees Azimuth	Heli	Jan 11, 2023	2,656	2,516
57	Level 0 Degrees Azimuth	Heli	Jan 11, 2023	2,592	2,489
58	Level +30 Degrees Azimuth (Not used for analysis)	Heli	Jan 11, 2023	2,586	2,447
59	Level -40 Degrees Azimuth	Heli	Jan 11, 2023	2,604	2,656
60	Level -40 Degrees Azimuth	Heli	Jan 11, 2023	2,595	2,752
61	Level -20 Degrees Azimuth	Heli	Jan 11, 2023	2,565	2,695
62	Level -25 Degrees Azimuth	Heli	Jan 11, 2023	2,601	2,677
63	Level -30 Degrees Azimuth	Heli	Jan 11, 2023	2,598	2,595
64	Level -50 Degrees Azimuth	Heli	Jan 11, 2023	2,577	2,789
65	Level -20 Degrees Azimuth	Heli	Jan 11, 2023	2,562	2,668
66	Level -55 Degrees Azimuth	Heli	Jan 11, 2023	2,589	2,604
67	Level -7 Degrees Azimuth	Heli	Jan 11, 2023	2,574	2,646
68	Level -90 Degrees Azimuth	Plane	Jan 16, 2023	2,653	2,571
69	Level -55 Degrees Azimuth	Plane	Jan 16, 2023	2,640	2,534
70	Level -5 Degrees Azimuth	Plane	Jan 16, 2023	2,646	2,441
71	Level -92 Degrees Azimuth	Plane	Jan 16, 2023	2,631	2,722
72	Level -75 Degrees Azimuth	Plane	Jan 16, 2023	2,625	2,746
73	Level -60 Degrees Azimuth	Plane	Jan 16, 2023	2,643	2,713
74	Level -20 Degrees Azimuth	Plane	Jan 16, 2023	2,610	2,801
75	Level -3 Degrees Azimuth	Plane	Jan 16, 2023	2,595	2,695
76	Level +5 Degrees Azimuth	Plane	Jan 16, 2023	2,601	2,771
77	Intentional Miss	Plane	Jan 16, 2023	2,656	2,749
78	Level -80 Degrees Azimuth	Plane	Jan 16, 2023	2,571	2,425
79	Level -50 Degrees Azimuth	Plane	Jan 16, 2023	2,586	2,556
80	Level +10 Degrees Azimuth	Plane	Jan 16, 2023	2,619	2,513

Appendix A contains details regarding the aircraft used in each sortie, the system configuration, weather data, test points, test notes, and flight paths for each test maneuver conducted over the airborne DAA flight campaign.

An example of the flight path diagrams is shown in Figure 24. The flight path figures are shown 'North Up' with the red path representing the intruder aircraft (Harvard or Bell 206), and the blue path representing the host Bell 205. All tracks shown are for the same time range. KML flight path and animation files are available in the NRC data repository.

It should be noted that the intercept azimuth angles are recorded in degrees from the host Bell 205's heading as opposed to velocity track. This decision was made since the DAA sensors under investigation all measure with respect to the host aircraft heading. Given that the azimuth measurement is with respect to heading it may appear as if the flight paths do not correspond to the recorded azimuth during cases where the host aircraft is highly crabbed owing to wind.

Figure 24: Example Flight Path from Intercept 15 -32 Degrees Azimuth (Blue - Bell 205, Red - Harvard)

7.0 DATA ANALYSIS – IRIS AUTOMATION CASIA X

Detailed results for each sortie are published separately as Appendix B. The summarized results analysis are repeated in this report for ease of comparison, and completeness.

The Casia X was serviceable, and properly configured for all 79 intercepts performed as part of this flight trial, however two intercepts involved sideslip crab angles resulting the intruder being outside the FOV. Table 4 below presents a summary of the intercepts performed including missed detections and false positives.

Table 4: Summary of Intercepts, Missed Detections and False Positives

	Total	Intruder Above	Intruder Below
Intercepts	77	59	18
Missed Detections	22	2	18
Missed Detections (%)	28.5	3.4	100.0
False Positives	0	0	0

From Table 4 it can be seen that the Casia X has been tuned to produce little to no false positives, however this has likely also resulted in a diminished ability to detect intruder aircraft located below the horizon. During the testing conducted by the NRC, at no time did the Casia X produce a detection when the intruder was below the horizon. It should be noted that while the DAA companion application computed the estimated sun elevation and azimuth, there was no attempt to structure the flight testing of the optical system into favourable, or unfavourable sun angle conditions. Moreover, since one of the conditions of the flight test plan was to ensure that visual contact was achieved prior to one nautical mile of separation no points were conducted with low sun elevation behind the intruder.

Table 5 presents a summary of the range, azimuth, and elevation errors calculated relative to the truth data collected by the host and intruder INSs. The table presents mean, and standard deviation measures for range at first detection, and range/azimuth/elevation error for all intercepts, and further broken down by intruder type (i.e. plane or helicopter). It should be noted that although standard deviation has been presented here, the distributions themselves do not necessarily appear Gaussian.

Table 5: Range, Azimuth, and Elevation Error

	All Intercepts		Helicopter		Airplane	
	Avg	Std	Avg	Std	Avg	Std
Range at First Detection (m)	1103	456	1042	328	1161	552
Range Error (m)	144	225	180	220	35	208
Azimuth Error (deg)	0.8	0.6	0.8	0.5	0.7	0.7
Elevation Error (deg)	-2.2	2	-2.3	1.9	-1.8	2.1

From Table 5 it can be seen that the average range at first detection is a little over one kilometer, with little variation between helicopter or airplane targets. The standard deviation of range at first detection is on the order of 500 meters, thus there is a significant degree of variability. The range, azimuth, and elevation error

show that there appeared to be some angular bias present in the implementation. It is possible that this was a result of slightly inaccurate camera extrinsic characteristics[2]. It is interesting to note, however, that the system appeared to produce more accurate results in azimuth as opposed to elevation, as the standard deviation of error is on the order of three times smaller. Estimation of range to a target from visual metrics alone is a difficult problem, and it is not surprising that the Casia X presents standard deviations of range error on the order of 200 meters. It is of interest to note that the average range error for the airplane target was small (35 m) compared to that of the helicopter (180 m). It is considered possible that for some of the helicopter intercepts that the target was improperly classified as an airplane, and thus employed a different scheme for estimating range. A cursory examination of the data available in the Iris Automation 'Flight Deck' interface did reveal that there were several times where the helicopter intruder was classified as a small plane. At present no further investigation has been conducted to validate this hypothesis.

Figure 25 presents a scatter plot of range at first detection for all intercepts that produced a valid detection. The solid red line presents the mean of 1103 meters, and the dashed red lines demonstrate the variance of one standard deviation about the mean.

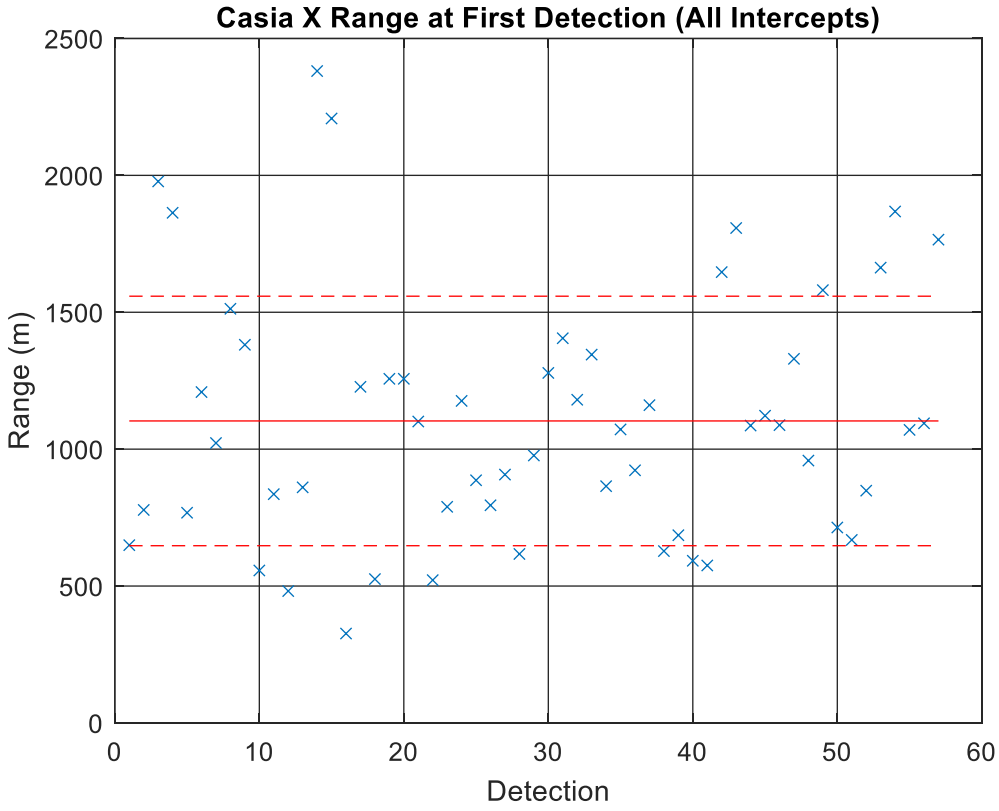

Figure 25: Range at First Detection vs Detection Number

[2] Camera extrinsic characteristics refer to the calibration of the camera axis and image plane with respect to the aircraft inertial frame.

Figure 26 presents a polar plot of range at first detection versus the average azimuth of the intercept as observed from the host aircraft (Bell 205). In the figure, the intercepts where the intruder was the helicopter (Bell 206) are shown by the blue circles, whereas those where the intruder was the airplane (Harvard Mk IV) are shown by the black crosses. No definitive trends are observable in this distribution of the data, however, it is hypothesized that there may be reduced detection range at the furthest extents of the Casia X field of regard (i.e. less than -90, or greater than +10 degrees azimuth in the NRC tested configuration). Investigation of this hypothesis has been left to a later date.

The top plot of Figure 27 presents the probability distribution histogram for range at first detection across all intercepts. The lower plot presents the cumulative probability distribution[3]. In each plot, the range at first detection has been binned and normalized count within the bin is represented on the vertical axis. The plot shows that highest concentration of first detections occur between 500 meters and 1300 meters, with a significant reduction in the probability as range increases beyond 1300 meters.

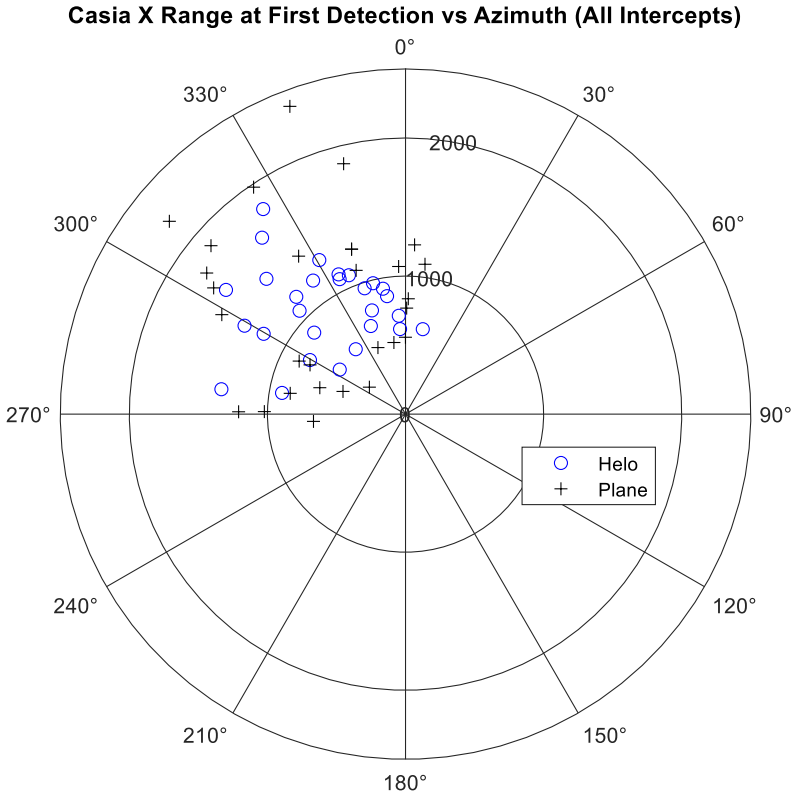

Figure 26: Range at First Detection vs. Azimuth

[3] The cumulative probability distribution plotted via the Matlab histogram function has an unintuitive interpretation. The blue bars can be seen as proportional to the probability that the target would be missed (i.e. not detected) within the given range bin.

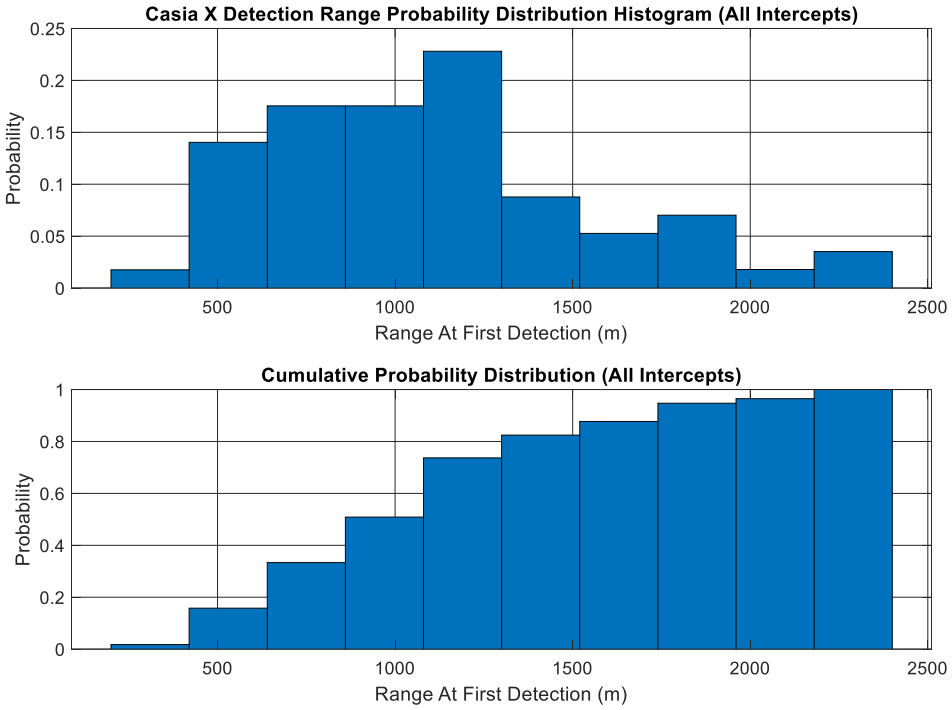

Figure 27: Detection Range Probability Distribution (All Intercepts)

The top plot of Figure 28 presents the range at first detection versus the rate of closure, with helicopter intruders as the blue circles, and the fixed wing intruder as black crosses. It can be seen that the cases with the fixed wing intruder involved higher closure rates, as expected. The middle plot of Figure 28 presents the total duration of time the intruder was tracked as a function of closing rate. From the plot it can be seen that most tracks had a duration of approximately 15 seconds, although tracks at very low closure rates could persist for 90 seconds and beyond. Figure 28 is worth consideration from the standpoint of practical implementation on board an RPA. It presents an indication of the need to make rapid decisions on board the RPA, as there is simply insufficient time available to telemeter data back to a GCS and have a human pilot make a decision to avoid. For example, at a detection range of 1100 meters and a closing rate of 85 meters per second, there is 13 seconds until the aircraft come into contact. Depending on the avoidance maneuver selected this may not even be sufficient time for an automated avoidance, let alone a manually initiated one. Further study into the efficacy of common avoidance algorithms given these realistic detection ranges/times is recommended. The lowest plot in Figure 28 presents the time prior to collision at first detection. On average first detection is achieved 22 seconds prior to predicted collision with a standard deviation of 14 seconds.

Figure 29 presents the horizontal position, range, azimuth, and elevation error history for all intercepts with valid detections. For these plots the data for each track was plotted as a function of true range. Each intercept was plotted with a different color in a cyclical sequence of: black, blue, red, green, cyan, magenta. The top plot presents the horizontal position error versus range. It should be noted that horizontal position error here includes the cumulative effects of azimuth, elevation, and range error, as well as ownship odometry errors as it is derived from the magnitude of difference between the estimated intruder and the truth data recorded by the INS installed on the intruder aircraft. The second plot of Figure 29 presents the range error as a function of range. It can be seen from this plot that range error is on the order of 200 meters on average out to about 1000 meters. Here the positive value of range error indicates that the Casia X has overestimated

the range to the intruder (i.e. it is closer than estimated). The overall trend in range error reverses above about 1200 meters. This may be a result of algorithmic tuning to detection ranges around 1000 meters. The over estimation of ranges below 1000 meters may be in part a result of classification errors (e.g. helicopter target classified as a plane).

The lower two plots of Figure 29 present the angular errors versus range. From these plots it can be seen that there is an average bias of approximately 1 degree in azimuth, and -2 degrees in elevation. The scatter in the elevation error appears to be much higher. The reason for this is presently unknown.

Figure 30 presents the error probability distribution as a series of histograms. The top plot shows the range error probability distribution in bins with a width of 5 meters. The second plot shows the azimuth error distribution in bins with a width of 0.5 degrees. The third plot presents the elevation error distribution in bins with a width of 0.5 degrees. The lowest plot presents the probability distribution histogram as a function of the duration of the track. These plots demonstrate that the Casia X system has excellent azimuthal accuracy, however elevation accuracy suffers somewhat. Range accuracy exhibits significant variability.

Figures 31-34 present error history and probability distribution for the helicopter and airplane intercepts respectively. The difference in the range error plots in Figure 30 and 31 seems to support the hypothesis that the helicopter range is over predicted below 1000 meters. By comparison, in Figure 31 the intercepts with the airplane as the intruder show the range error as more centered around 0 when compared with the helicopter intercepts of Figure 31.

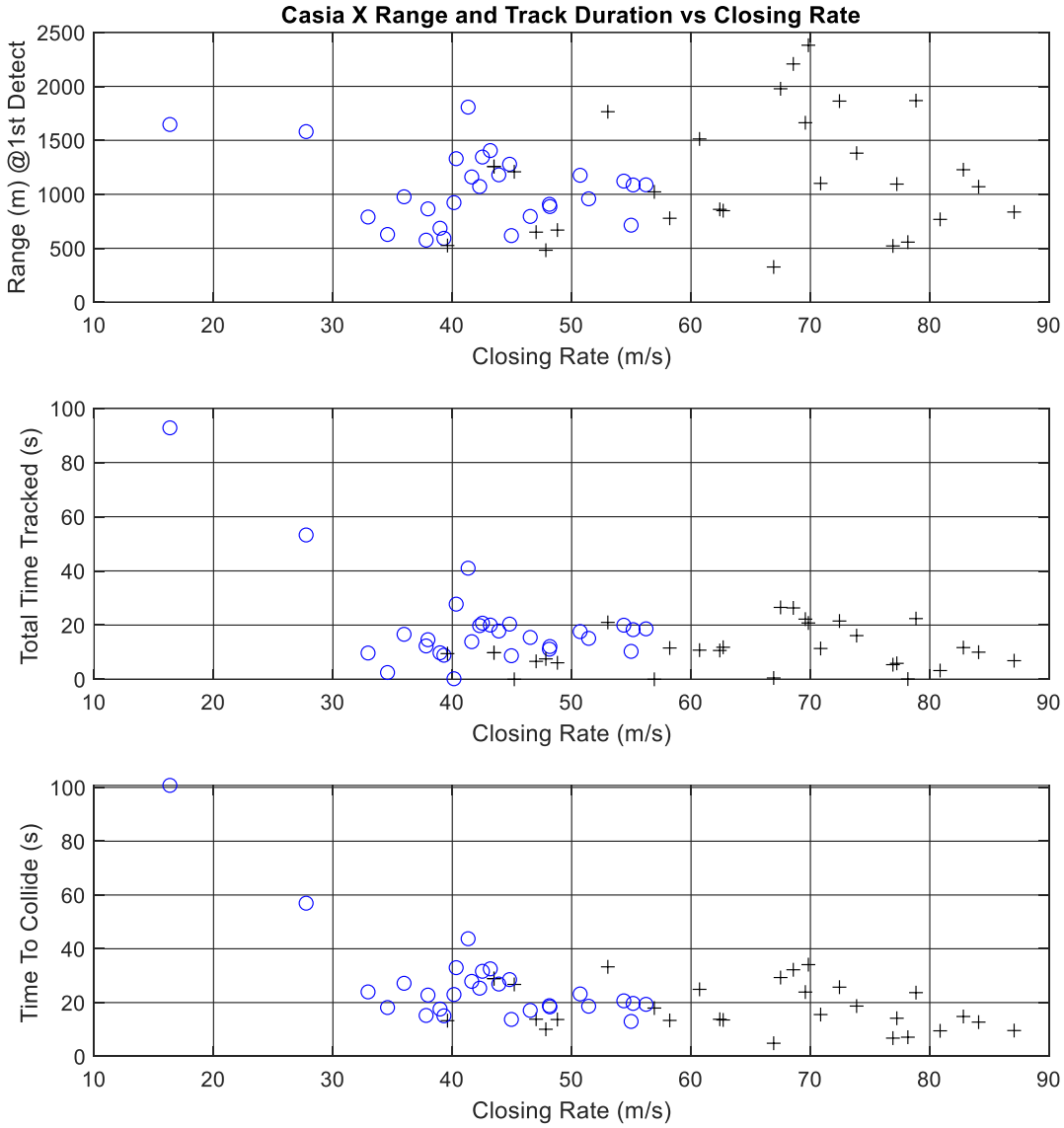

Figure 28: Range at first Detection and Track Duration vs. Closing Rate

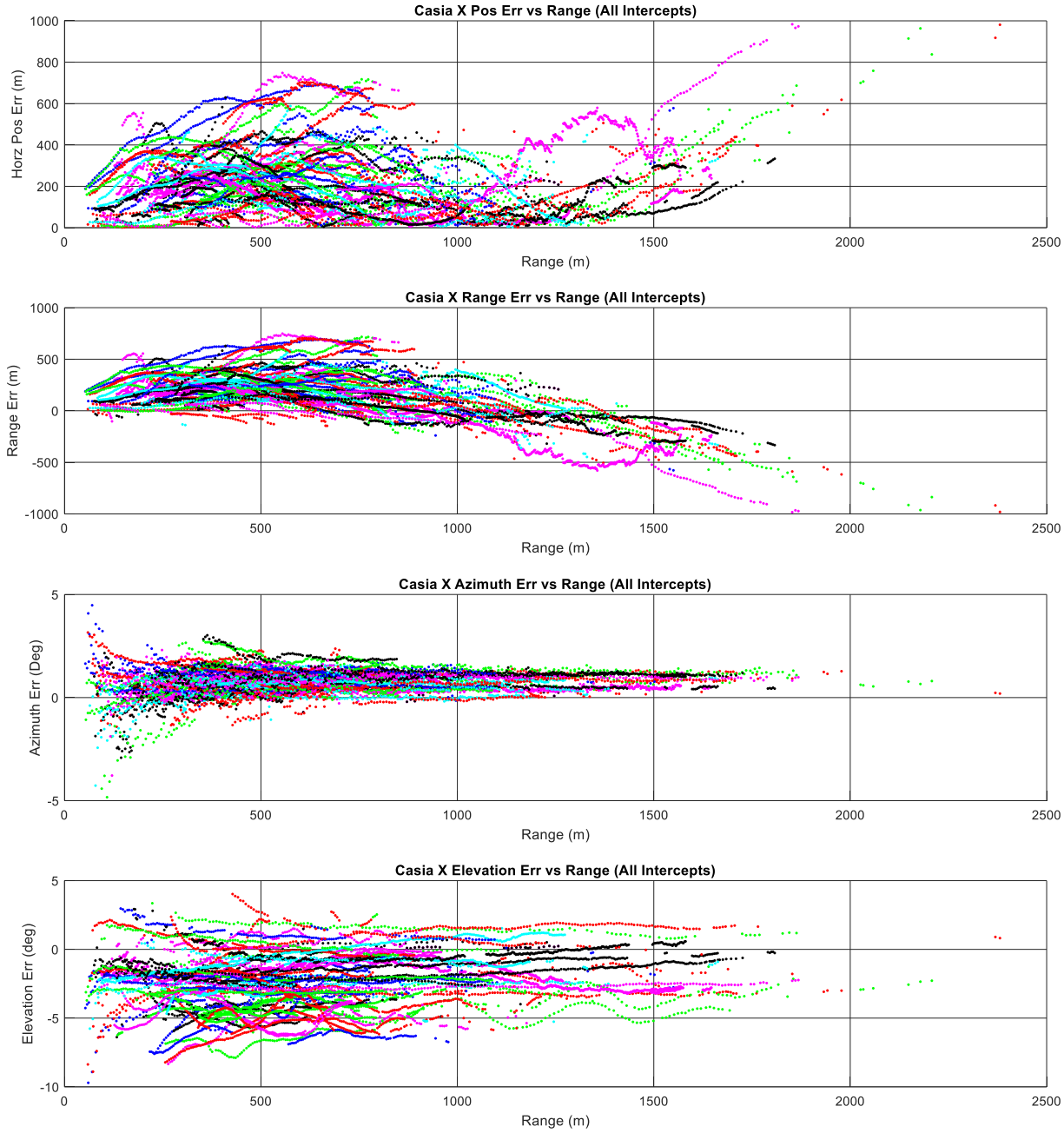

Figure 29: Error History (All Intercepts)

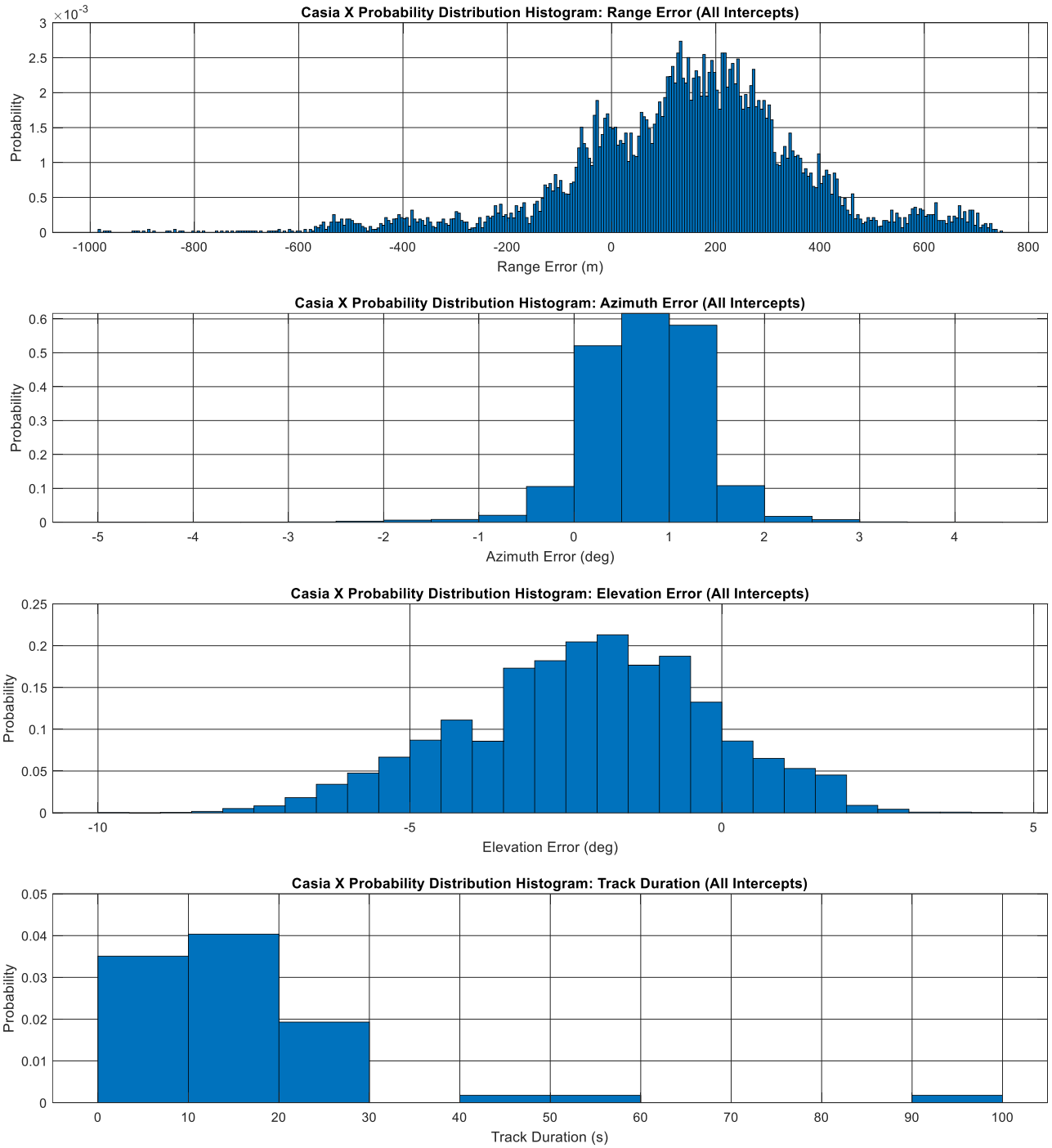

Figure 30: Error Distribution (All Intercepts)

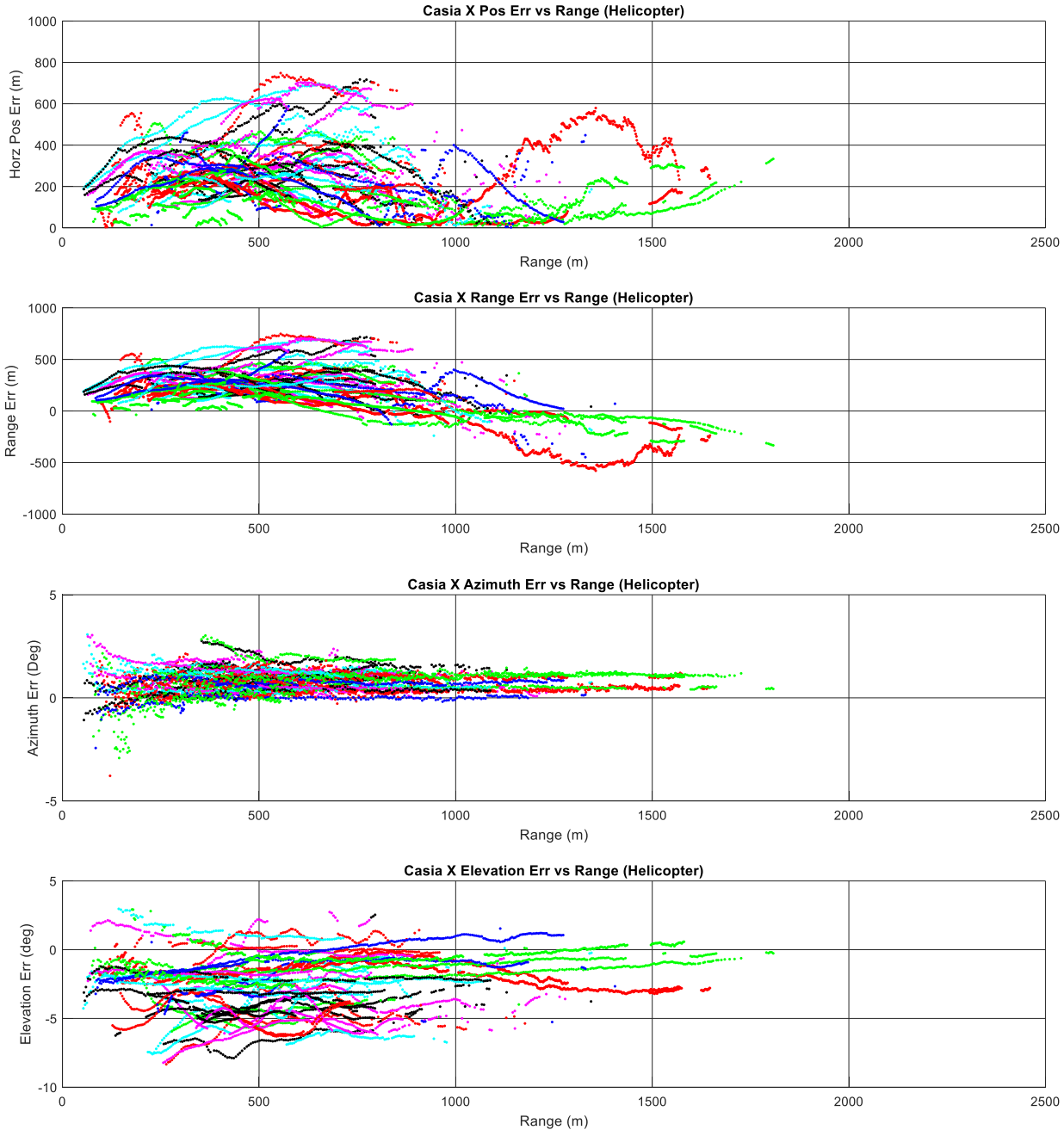

Figure 31: Error Distribution (Helo)

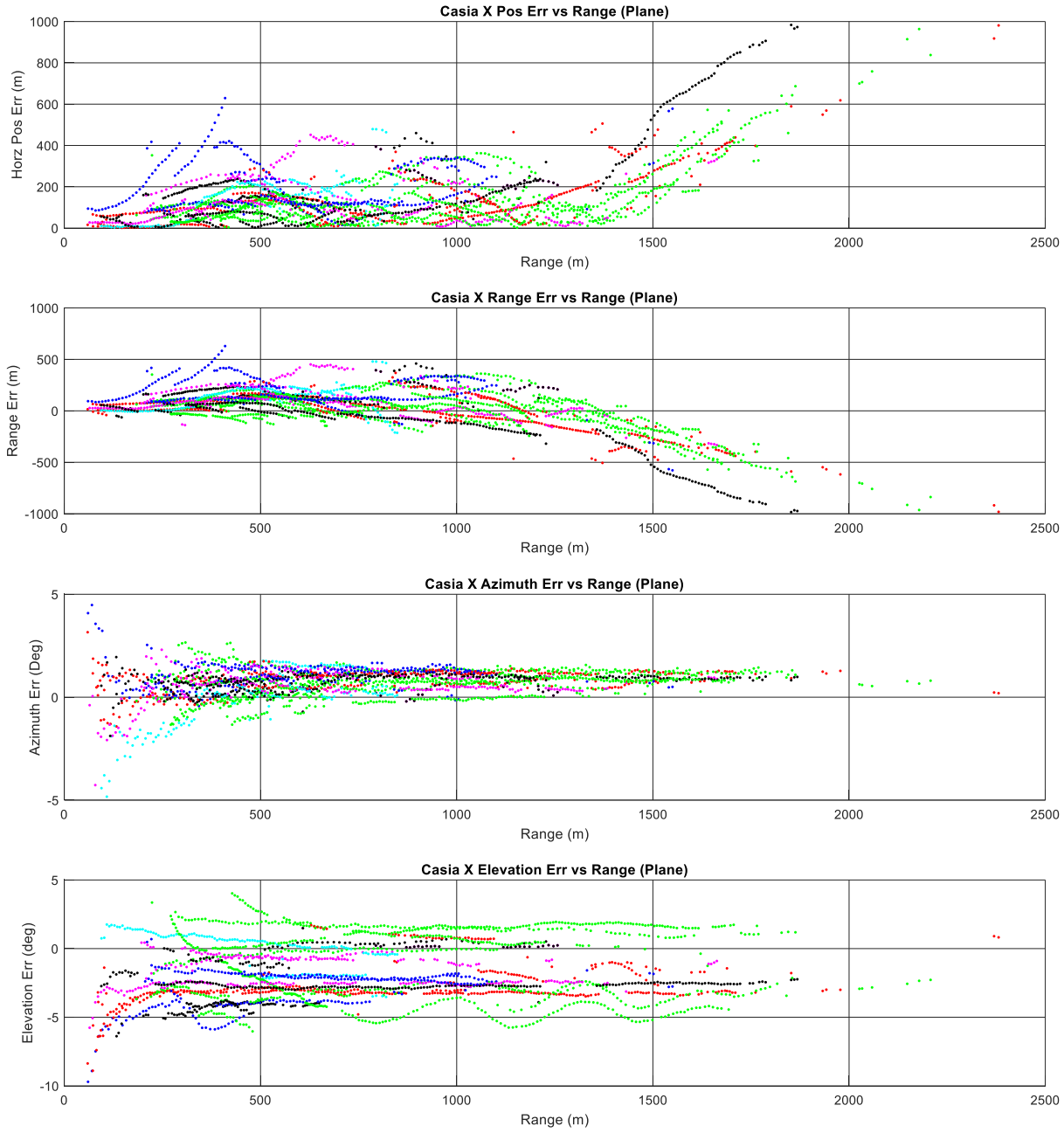

Figure 32: Error Distribution (Plane)

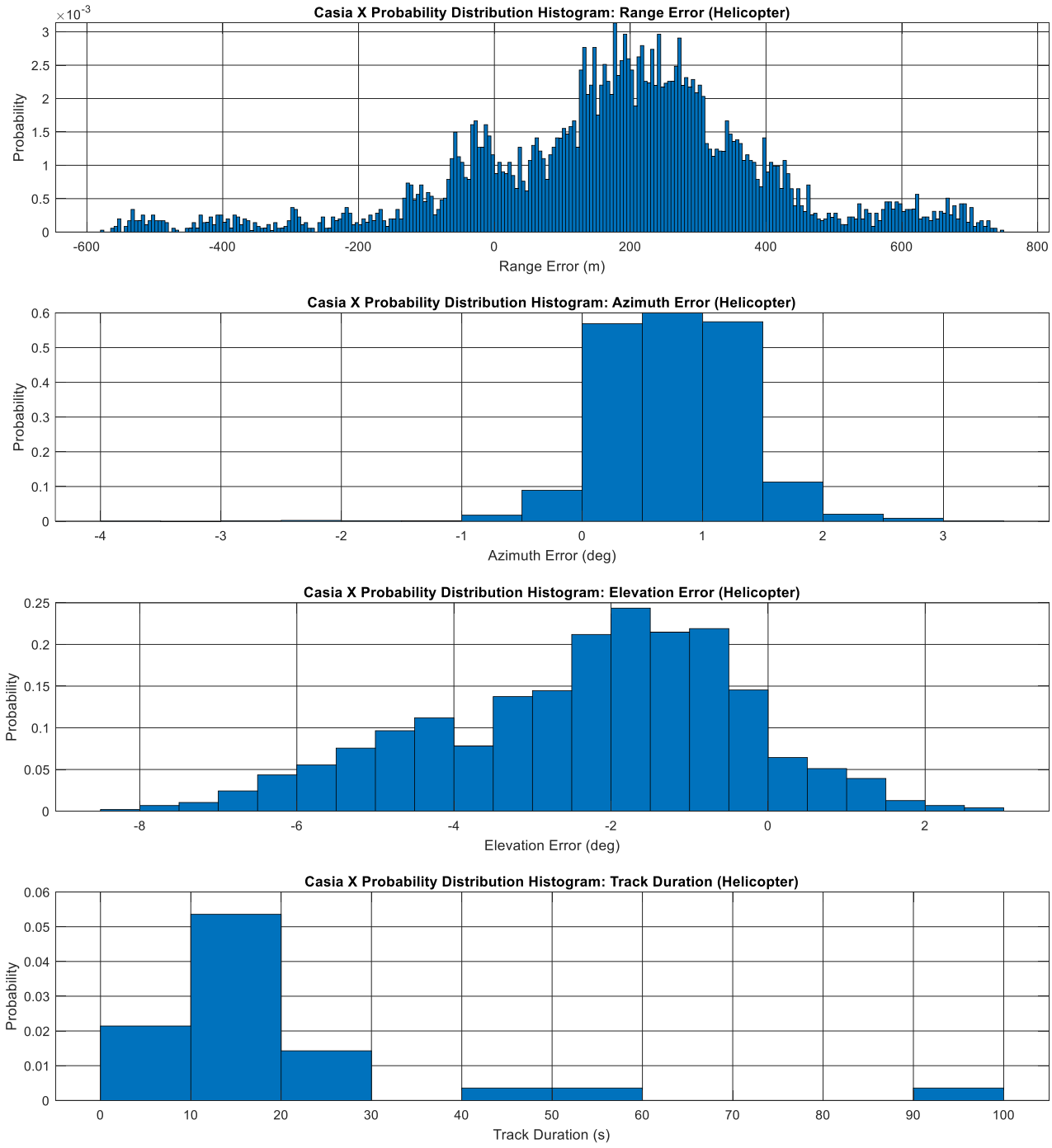

Figure 33: Error Distribution Histograms (Helicopter)

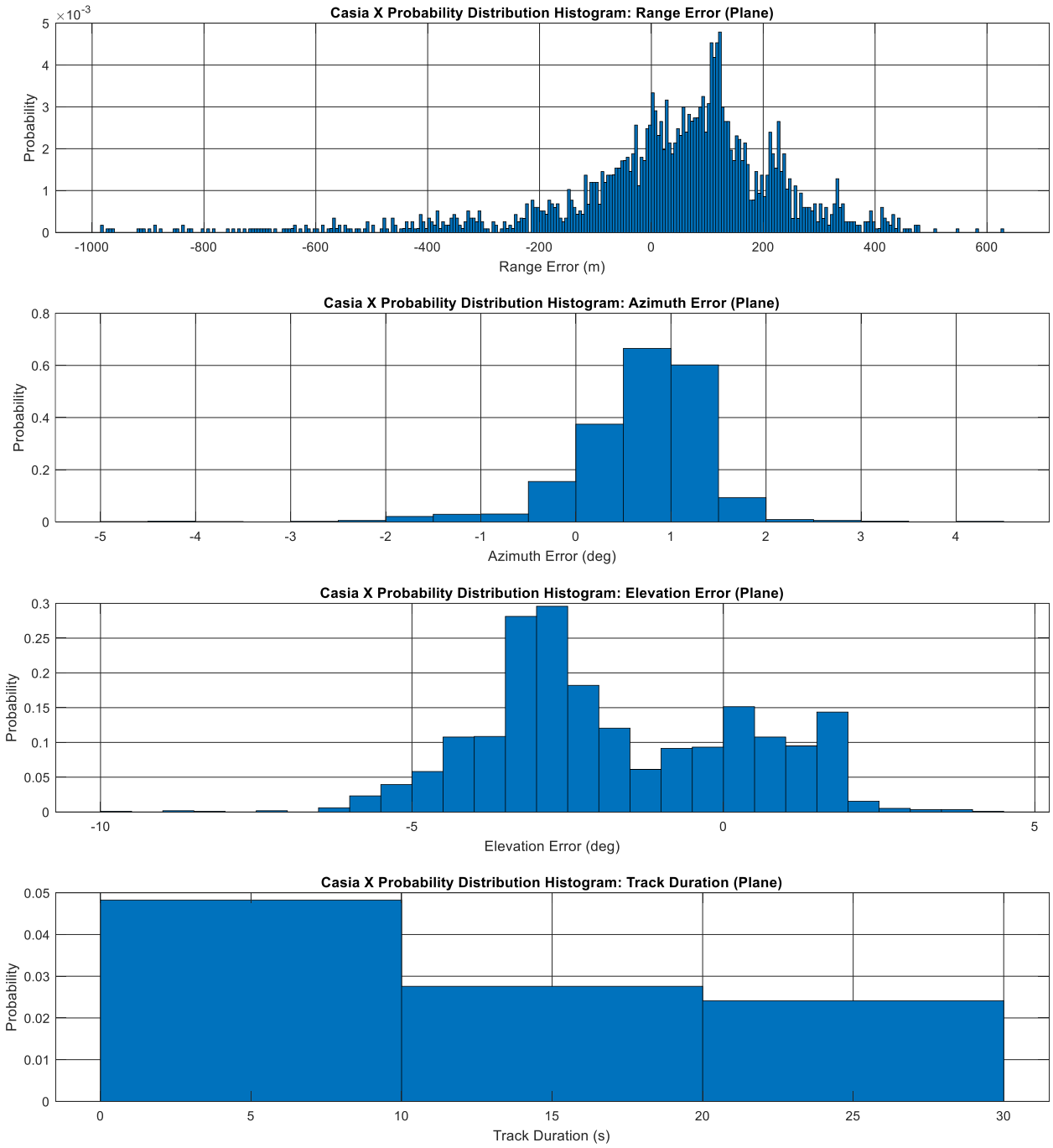

Figure 34: Error Distribution Histograms (Plane)

7.1 Manufacturer Comment

Iris Automation was provided an advance copy of the results in Appendix B for comment. This section contains their response.

Iris Automation Inc. (now a part of uAvionix Corporation) is extremely pleased with the results of

this testing, and the conclusions made by the team at the NRC in this report. Overall, the report matches our internal, and third party, performance evaluations of the Casia system to within an error bound that we would expect. This additional testing further serves to confirm the validity of those results and highlight Casia as a leading vision based airborne and ground based aircraft detection and tracking system. We would like to highlight some areas of additional context for the reader, discussed below.

Advantages of a Vision System

We would like to highlight that the report was created using data gathered from v2.4 of the FlightCore software that runs on the Casia device, which was originally released in May of 2022. One of the great advantages of Casia, and vision systems in general, is that as the software improves so does the system performance without any change in hardware. Our latest version of software (v3.4 released in November 2023) includes dramatic improvements in detection rate, detection range, and many other metrics.

Another advantage of the vision based approach used in Casia is the accuracy and rapid update rate of the vector to the target intruder aircraft. Unlike RADAR systems, vision technology can generate sub-degree accurate vectors to objects seen within the imagery at a high update rate, as shown in the results of this report. The accuracy and timeliness of this data is extremely beneficial when performing integration with other systems as it makes the job of data fusion much simpler.

Lastly, we would like to highlight the benefit of class identification of intruder aircraft. Other detection technologies struggle with being able to provide additional context or information to the user about the detection object, however with the knowledge of the intruder object type operators and users and systems can make faster and more informed decisions with the data.

Challenges with Vision Systems

The report highlighted the low detection rates of aircraft that are flying below the ownship, with ground clutter behind the intruder aircraft. This is a known limitation of vision systems (similar to other detection systems/methods) and something that Iris Automation has invested heavily in improving. In later versions of our software released since the testing took place a significant improvement in the detection rate of aircraft flying in front of background clutter has been made, and will continue to be made as software enhancements are developed.

Integration Notes

It was noted that the Casia system under test is limited by the MAVLink ADS-B Vehicle message being used to transmit data from Casia as it can only communicate in global positional coordinates rather than the more accurate angular coordinates. We would like to note that the device has other real-time output interfaces and protocols that include this more accurate data, however due to the nature of the open source MAVLink protocol, autopilot systems, and groundstation systems that it was designed to integrate into, this data wasn’t able to be output over the interface used in the testing.

8.0 DATA ANALYSIS – ECHODYNE ECHOFLIGHT

Detailed results for each sortie are published separately as Appendix C. The summarized results analysis are repeated in this report for ease of comparison, and completeness.

The data acquisition system recorded track data packets as reported from the EchoFlight radar, and time stamped them upon arrival allowing for downstream post processing to be performed. The EchoFlight track data recorded azimuth, elevation, and slant range in local coordinates, requiring the use of host aircraft attitude and position measurements to transform the data to world referenced (e.g. Latitude/Longitude) coordinates. This was performed via the following process:

1. Host and Intruder positions, velocities and attitudes as recorded by their inertial navigation systems were trimmed to a common time span and interpolated to a common 100 Hz time base.
2. EchoFlight Azimuth and Elevation data was compensated for the installation angles (40 degrees in azimuth, and 4 degrees elevation), and adjusted for sign convention.
3. Host INS data was converted to UTM coordinates
4. Host position and attitude were linearly interpolated to the reported time of each EchoFlight track data packet.
5. Track range, azimuth, and elevation data was converted to cartesian x, y, z values in meters
6. The x, y, and z values from step 5 above were added to the Host UTM position and altitude (in meters) to establish the estimated world coordinate location of the intruder
7. System time stamps were used to interpolate Host and Intruder data to the time at which tracks were received from the EchoFlight system. The following parameters were calculated at this time for each track:
    a. UTM position of Host and Intruder as reported by their INS
    b. UTM position of the Intruder as determined from steps 2-6 above
    c. Horizontal position error of the Intruder
    d. Range to Intruder, and range error
    e. Azimuth, and Elevation to Intruder, and error

The EchoFlight was nominally configured for detections over a wide azimuth and for long range performance. Given that the flight testing took place at altitudes as low as 2000 ft AGL, and the host aircraft pitch and roll attitude varied in response to prevailing wind a number of false positive tracks from strong ground reflections were generated. A process was developed, and detailed in Appendix C for removing ground reflections and false tracks to facilitate the data analysis. To assist in the determination of which track ID's were associated with valid detections an algorithm was developed to filter tracks based on range and azimuth error as calculated relative to the truth data provided by the INS installed on board the intruder. Such a technique is only possible in post-processing with a suitable source of truth data available, and is only intended to allow for an assessment of the available performance of the EchoFlight. In practice track filtering routines would need to be developed, or further refinements to the radar parameters would be required to reduce the number of false positives.

Over the course of flight testing several configuration changes were made to the EchoFlight in effort to reduce the number of false positives. One of these configuration changes resulted in a typo being entered in the parameter list which ultimately prevented the radar from acquiring tracks below an elevation of 5 degrees. Flights affected by this typo (August 5th, 10th and 11th 2022) were removed from the comprehensive data analysis. It is noted that the lack of consistency in radar configuration introduces variability in the interpretation of the results.

The EchoFlight was serviceable, and properly configured for 49 of the 77 intercepts selected for analysis as part of this flight trial. Table 6 below presents a summary of the intercepts performed including missed detections and false positives.

Table 6: Summary of Intercepts, Missed Detections and False Positives

	Total	Intruder Above	Intruder Below
Intercepts	49	35	8
Missed Detections	10	9	1
Missed Detections (%)	20.4	25.7	12.5
False Positives	2812	N/A	N/A

From Table 6 it can be seen that the EchoFlight generated a significant number of false positives, highlighting the requirement to tune radar to reduce the impact of false positives. Detection performance was comparable for both above the horizon and below the horizon conditions.

Table 7 presents a summary of the range, azimuth, and elevation errors calculated relative to the truth data collected by the host and intruder INSs. The table presents mean, and standard deviation measures for range at first detection, and range/azimuth/elevation error for all intercepts, and further broken down by intruder type (i.e. plane or helicopter). It should be noted that although standard deviation has been presented here, the distributions themselves do not necessarily appear Gaussian.

Table 7: Range, Azimuth, and Elevation Error

	All Intercepts		Helicopter		Airplane	
	Avg	Std	Avg	Std	Avg	Std
Range at First Detection (m)	1990	1019	1684	1036	2705	501
Range Error (m)	-5	12	-5	11	-5	12
Azimuth Error (deg)	1.3	8.9	1.1	9.1	1.5	8.6
Elevation Error (deg)	-2.8	8.6	-3.7	8.6	-0.2	7.9

From Table 7 it can be seen that the average range at first detection is a little under two kilometers, with the airplane target being detected at a greater average range than the helicopter. This is likely reflective of the difference between radar cross section between the two aircraft. The standard deviation of range at first detection is on the order of one kilometer, thus there is a significant degree of variability. The range, azimuth, and elevation error show that there appeared to be some angular bias present in the implementation. It is possible that this was a result of slightly inaccurate boresighting measurements. The variability of the angular error was on the order of 9 degrees.

Figure 35 presents a scatter plot of range at first detection for all intercepts that produced a valid detection. The solid red line presents the mean of 1990 meters, and the dashed red lines demonstrate the variance of one standard deviation about the mean.

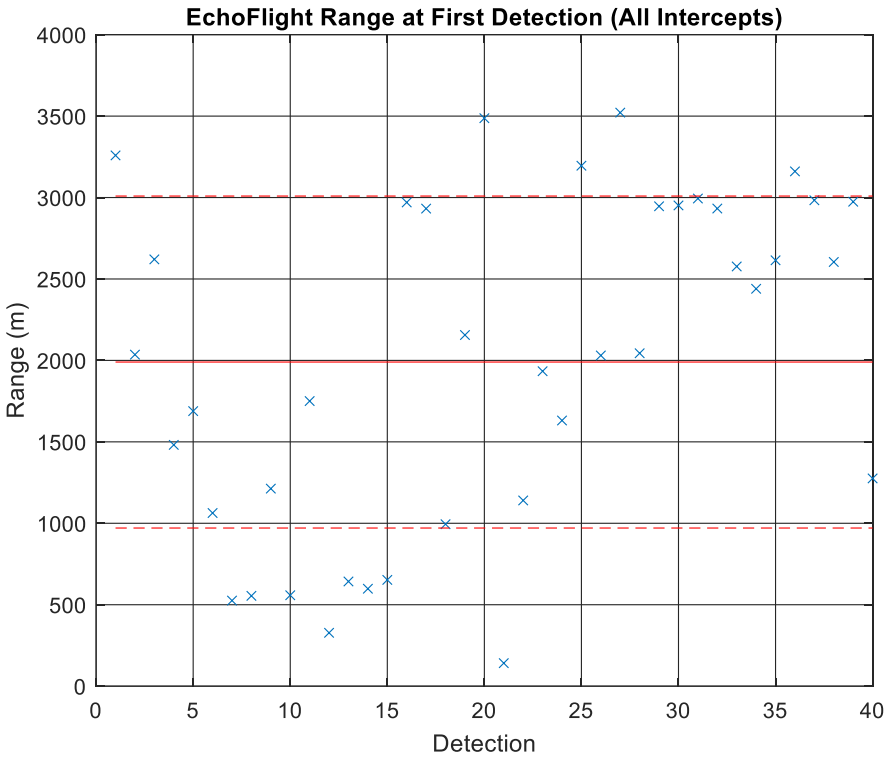

Figure 35: Range at First Detection vs Detection Number

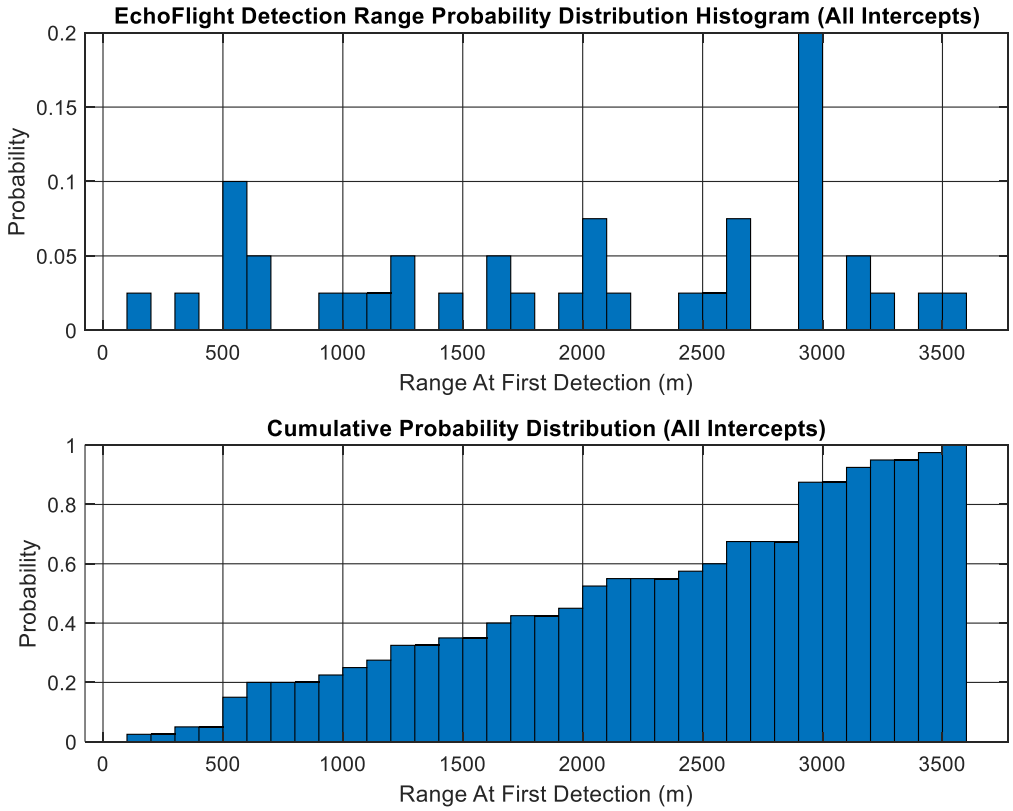

Figure 36: First Detection Range Probability Distribution Histogram

The top plot of Figure 36 presents the probability distribution histogram for range at first detection across all intercepts. The lower plot presents the cumulative probability distribution[4]. In each plot, the range at first detection has been binned and normalized count within the bin is represented on the vertical axis. The plot shows that first detection ranges were fairly equally distributed across the range from 500 to 3500 meters. This is also represented in the cumulative plot as a near linear rise in cumulative probability with increasing range.

Figure 37 presents a polar plot of range at first detection versus the average azimuth of the intercept as observed from the host aircraft (Bell 205). In the figure, the intercepts where the intruder was the helicopter (Bell 206) are shown by the blue circles, whereas those where the intruder was the airplane (Harvard Mk IV) are shown by the black crosses. No obvious trends are discernable from this plot, however it does appear that the helicopter was not detected when azimuth was less than approximately 295 degrees; however only two test cases satisfy that condition.

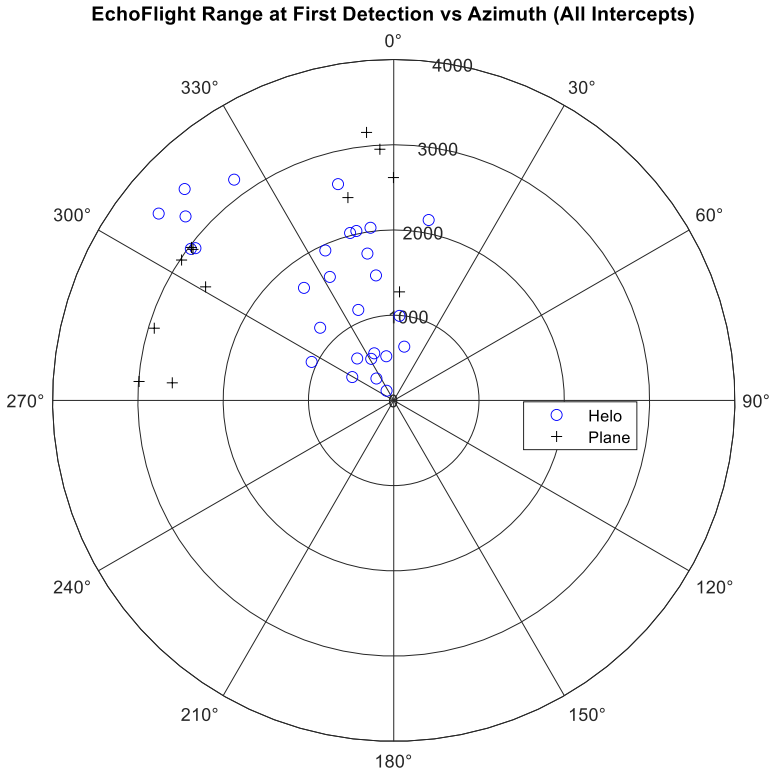

Figure 37: Range at First Detection vs Azimuth

[4] The cumulative probability distribution plotted via the Matlab histogram function has an unintuitive interpretation. The blue bars can be seen as proportional to the probability that the target would be missed (i.e. not detected) within the given range bin.

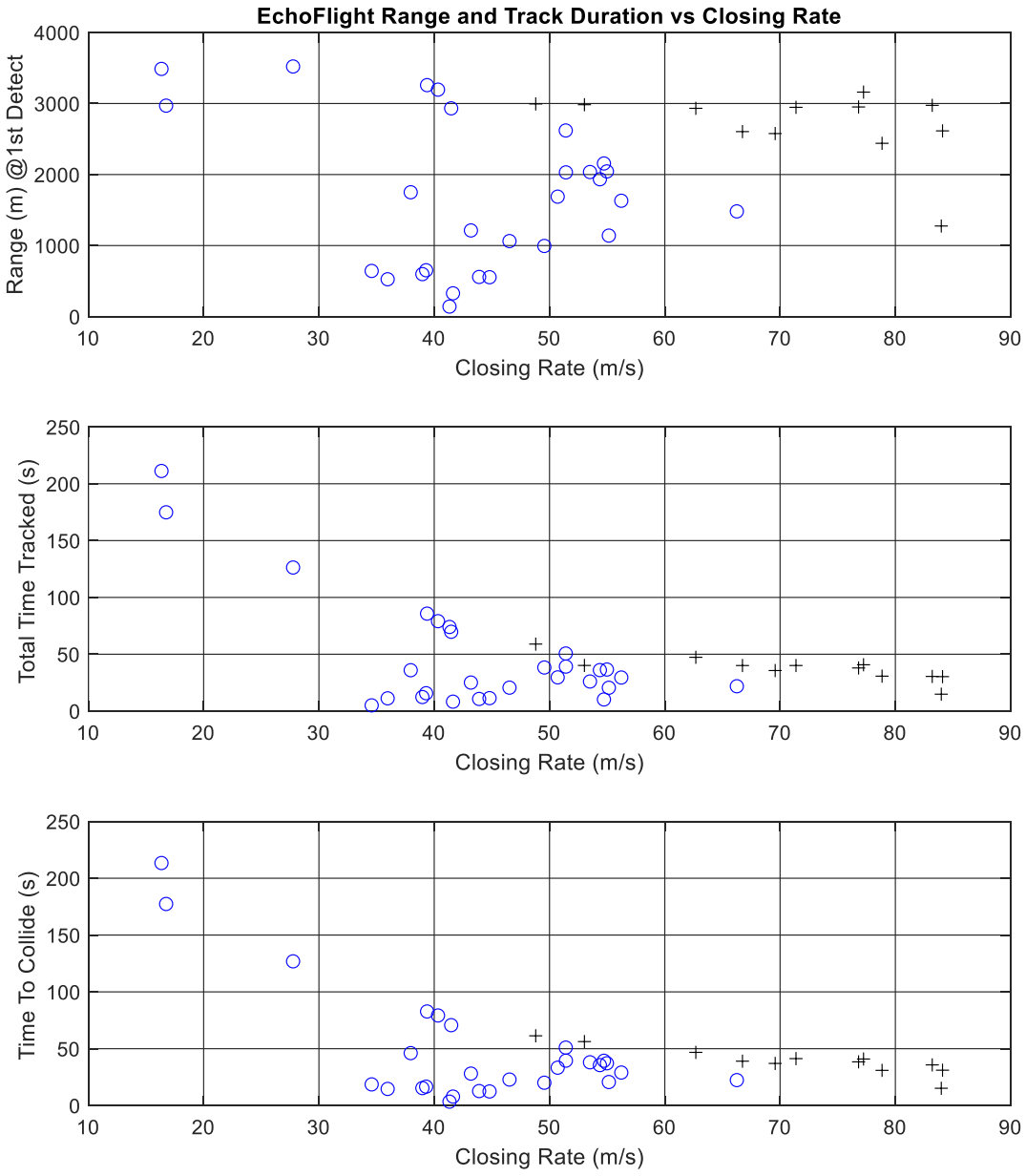

Figure 38: Range and Time Tracked vs Closing Rate

The top plot of Figure 38 presents the range at first detection versus the rate of closure, with helicopter intruders as the blue circles, and the fixed wing intruder as black crosses. It can be seen that the cases with the fixed wing intruder involved higher closure rates, as expected. The middle plot of Figure 38 presents the total duration of time the intruder was tracked as a function of closing rate. From the plot it can be seen that most tracks had a duration of approximately 40 seconds, although tracks at very low closure rates could persist for 125 seconds and beyond. Figure 38 is worth consideration from the standpoint of practical implementation on board an RPA. It presents an indication of the need to make rapid decisions on board the RPA, as there is likely insufficient time available to telemeter data back to a GCS and have a human

pilot make a decision to avoid. For example, at a detection range of 2500 meters and a closing rate of 85 meters per second, there is 30 seconds until the aircraft come into contact. If the system were to require manual selection of an appropriate maneuver this could involve significant human factors delays to assess the situation, select a maneuver, and issue the command to the vehicle.

Further study into the efficacy of common avoidance algorithms given these realistic detection ranges/times is recommended. The lowest plot in Figure 38 presents the time prior to collision at first detection. On average first detection is achieved 43 seconds prior to predicted collision with a standard deviation of 40 seconds indicating significant variability.

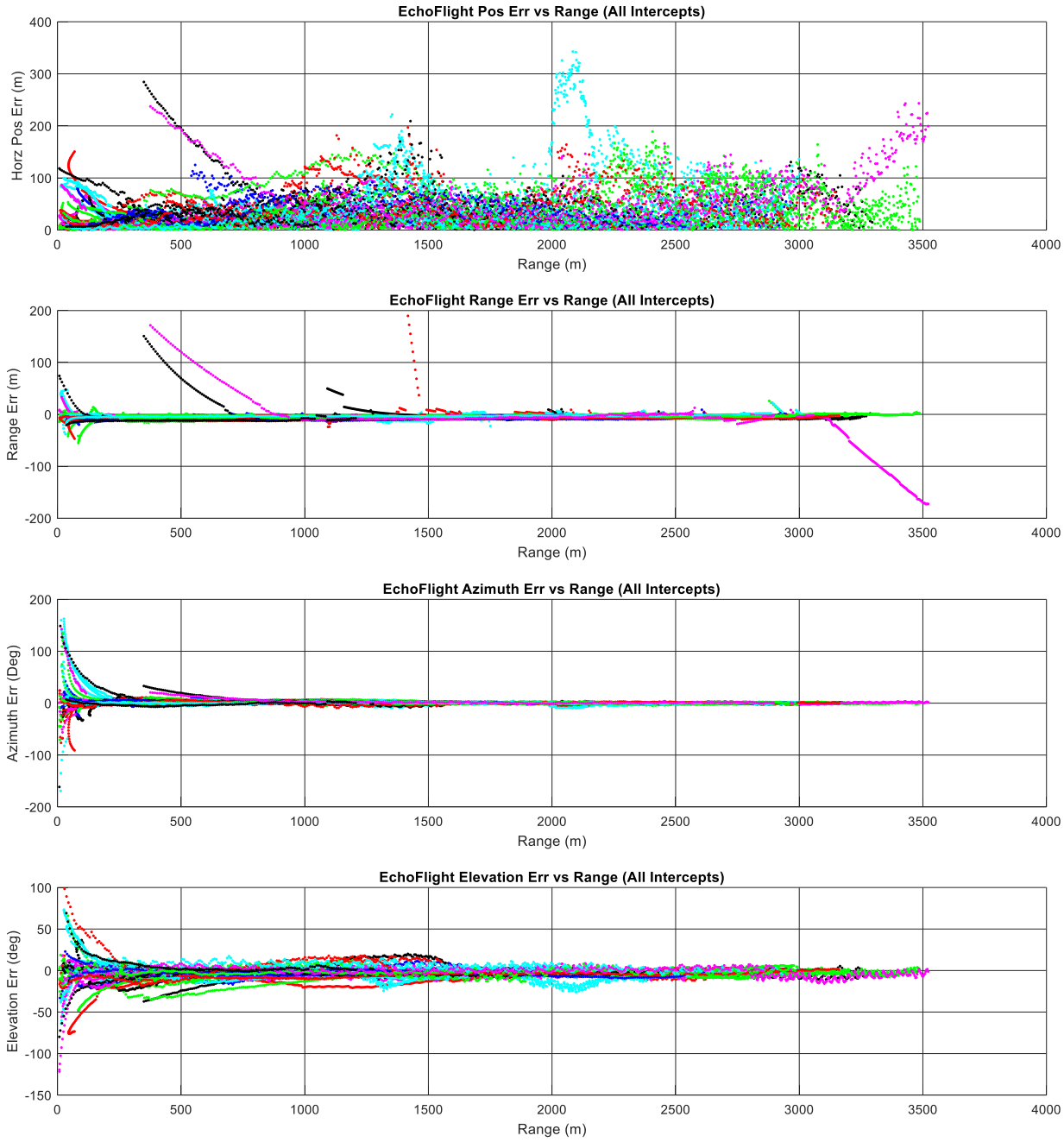

Figure 39: Error vs Range (All Intercepts)

Figure 39 presents the horizontal position, range, azimuth, and elevation error history for all intercepts with valid detections. For these plots the data for each track was plotted as a function of true range. Each intercept was plotted with a different color in a cyclical sequence of: black, blue, red, green, cyan, magenta. The top plot presents the horizontal position error versus range. It should be noted that horizontal position error here includes the cumulative effects of azimuth, elevation, and range error, as well as ownship odometry errors as it is derived from the magnitude of difference between the estimated intruder and the truth data recorded by the INS installed on the intruder aircraft. The second plot of Figure 39 presents the range error as a function of range. It can be seen from this plot that range error is typically small for valid tracks, but can drift to develop into significant values exceeding 100 meters. It is suspected that these cases (e.g. magenta and black traces in Figure 39) occur when the track has lost detection and is being extrapolated, or alternatively if the track has become split. It should be noted that split tracks were not processed specially in this analysis; i.e. any valid track was considered, even if at some point in time during the intercept the track became non-valid.

The lower two plots of Figure 39 present the angular errors versus range. From these plots it can be seen that there is an average bias of approximately 1 degree in azimuth, and -3 degrees in elevation. The scatter in the elevation error appears to be much higher. It is suspected that this is related to the larger bin sizes in the vertical axis of the EchoFlight radar.

Figure 40 presents the error probability distribution as a series of histograms. The top plot shows the range error probability distribution in bins with a width of 5 meters. The second plot shows the azimuth error distribution in bins with a width of 0.5 degrees. The third plot presents the elevation error distribution in bins with a width of 0.5 degrees. The lowest plot presents the probability distribution histogram as a function of the duration of the track. These plots demonstrate that the EchoFlight system as tested presented excellent range accuracy with a standard deviation on the order of 12 meters. Azimuthal and Elevational accuracy is more variable with a standard deviation on the order of 9 degrees.

Figures 41-44 present error history and probability distribution for the helicopter and airplane intercepts respectively. The plots show that the horizontal position error is primarily driven by variations in the azimuthal accuracy as the range errors appear to be significantly less than the horizontal position errors. The plots also appear to show that there is greater horizontal position error with the helicopter target. It is uncertain if this is due to differences in radar cross section, or simply a result of the flight testing conducted with the helicopter, where there were intercepts conducted at low altitudes above ground creating more opportunity for the radar to split tracks and generate detections from ground clutter.

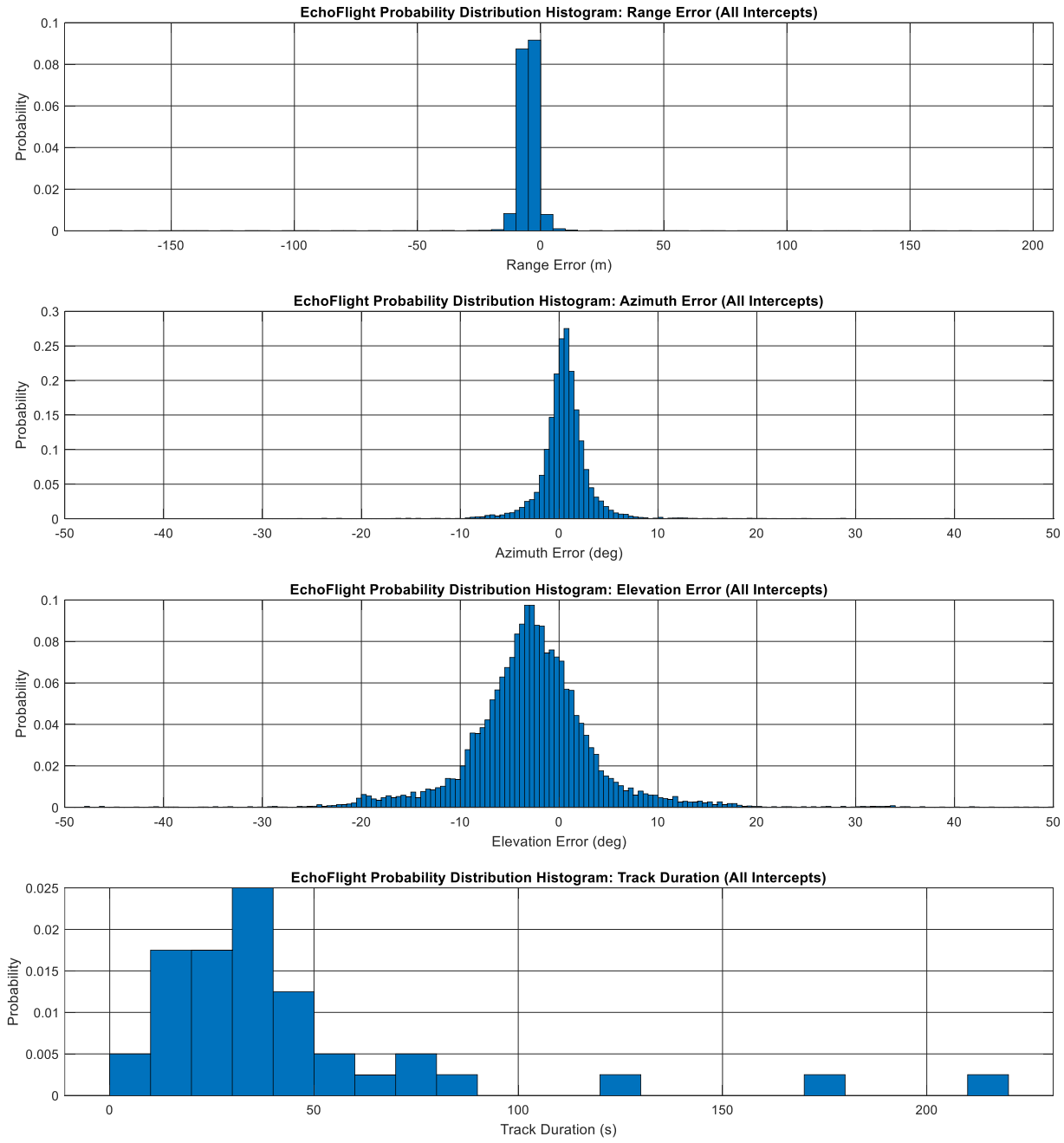

Figure 40: Error Probability Distribution Histograms (All Intercepts)

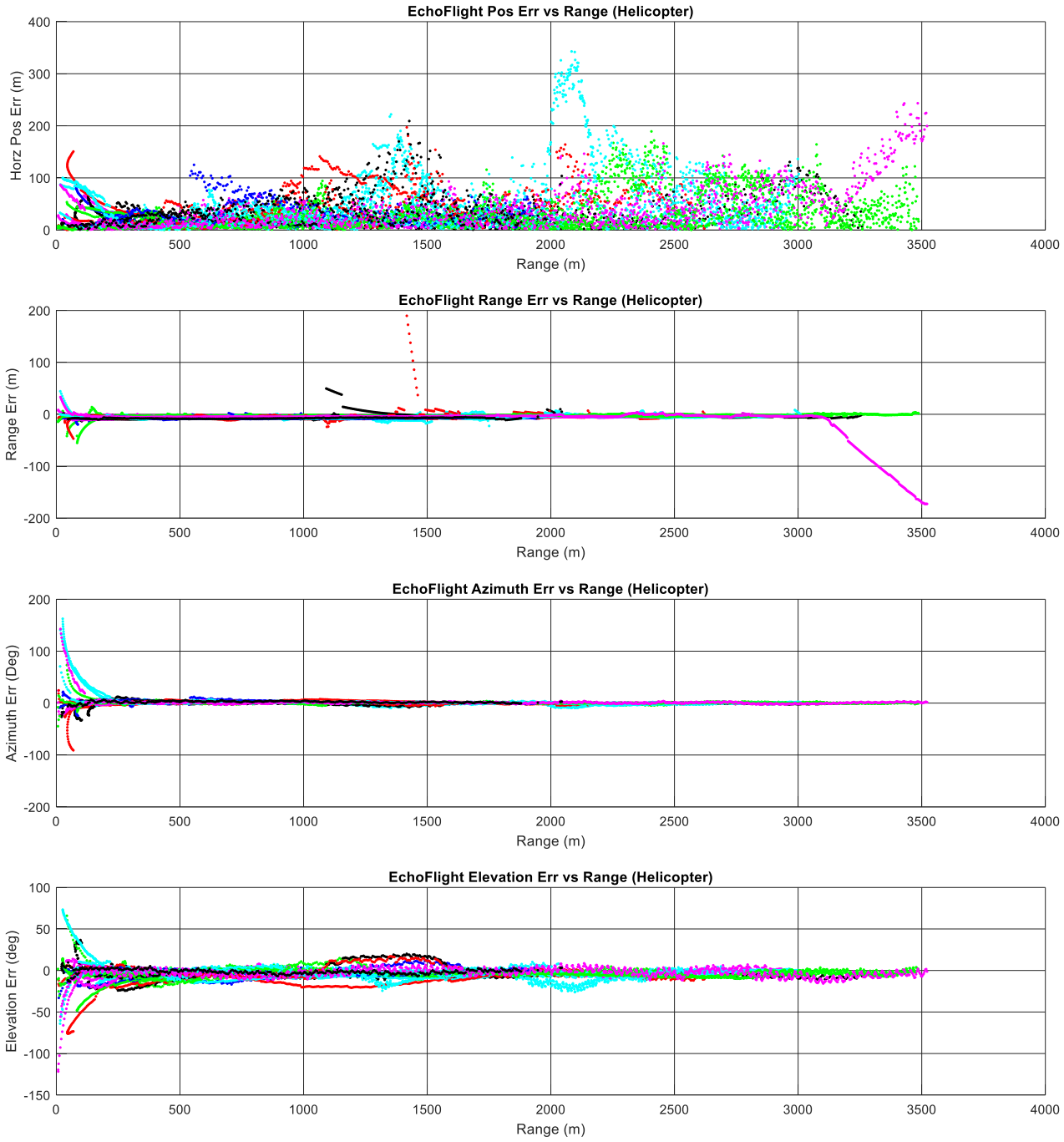

Figure 41: Error vs. Range (Helicopter)

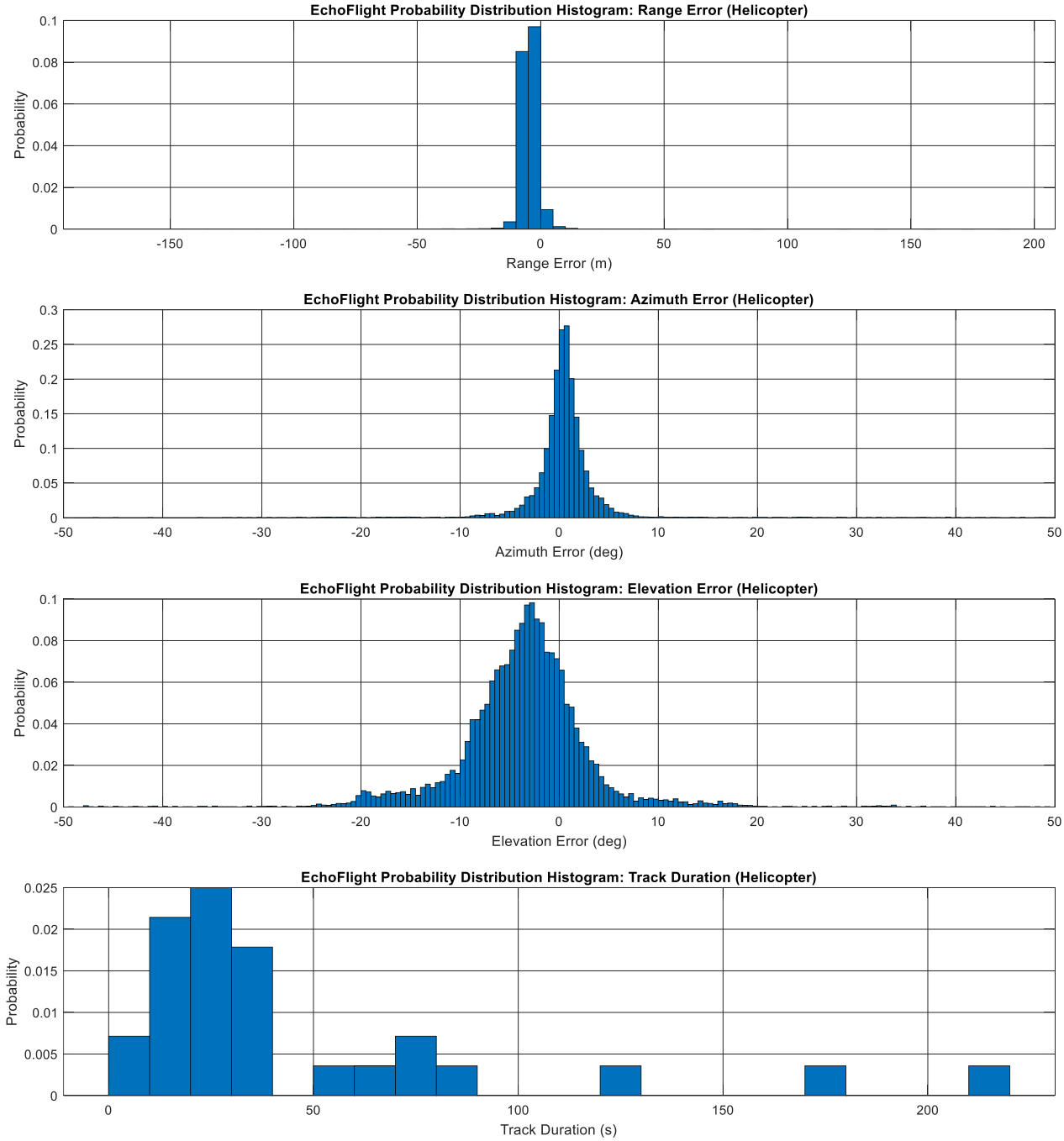

Figure 42: Error Probability Distribution Histograms (Helicopter)

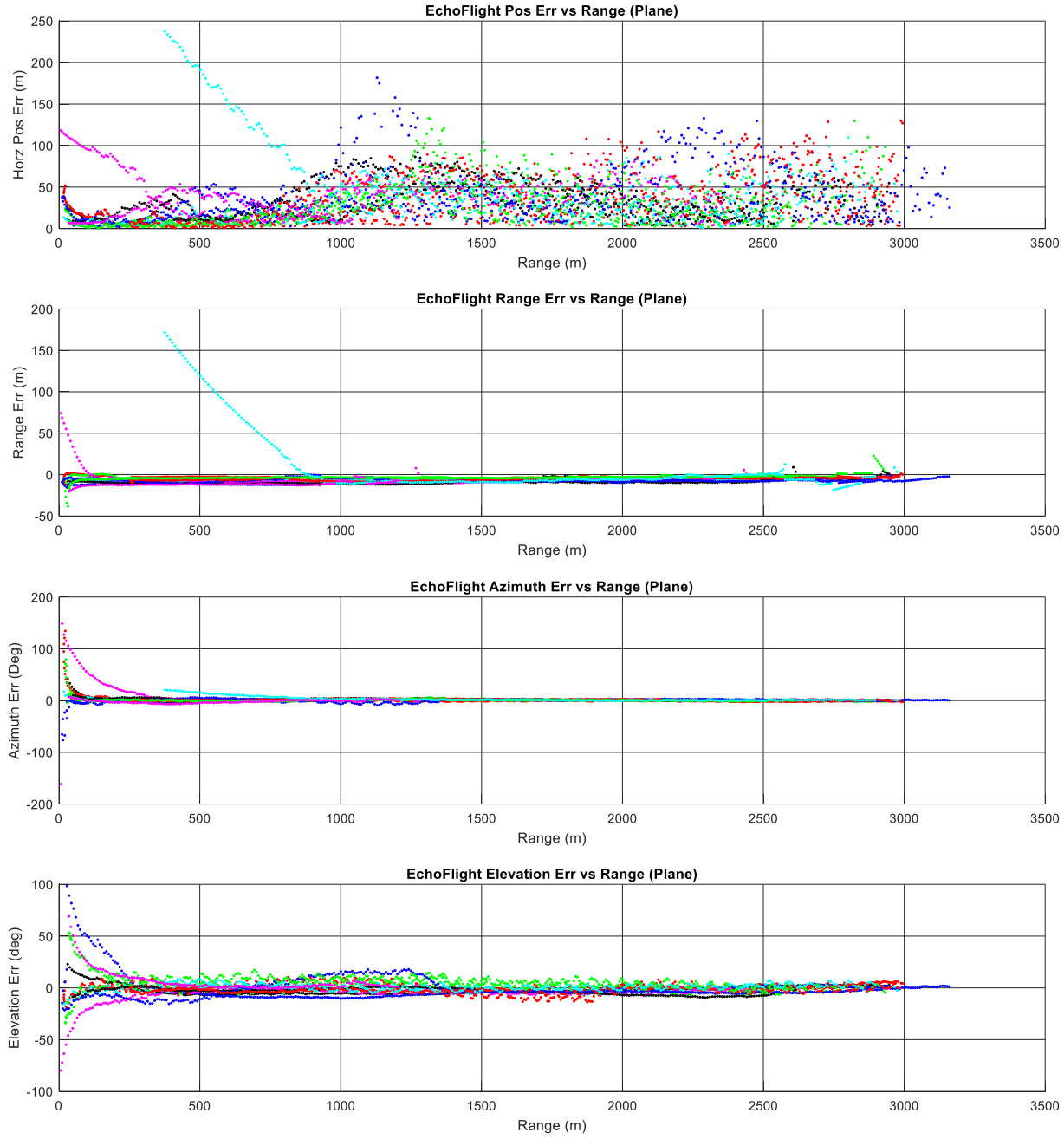

Figure 43: Error vs Range (Plane)

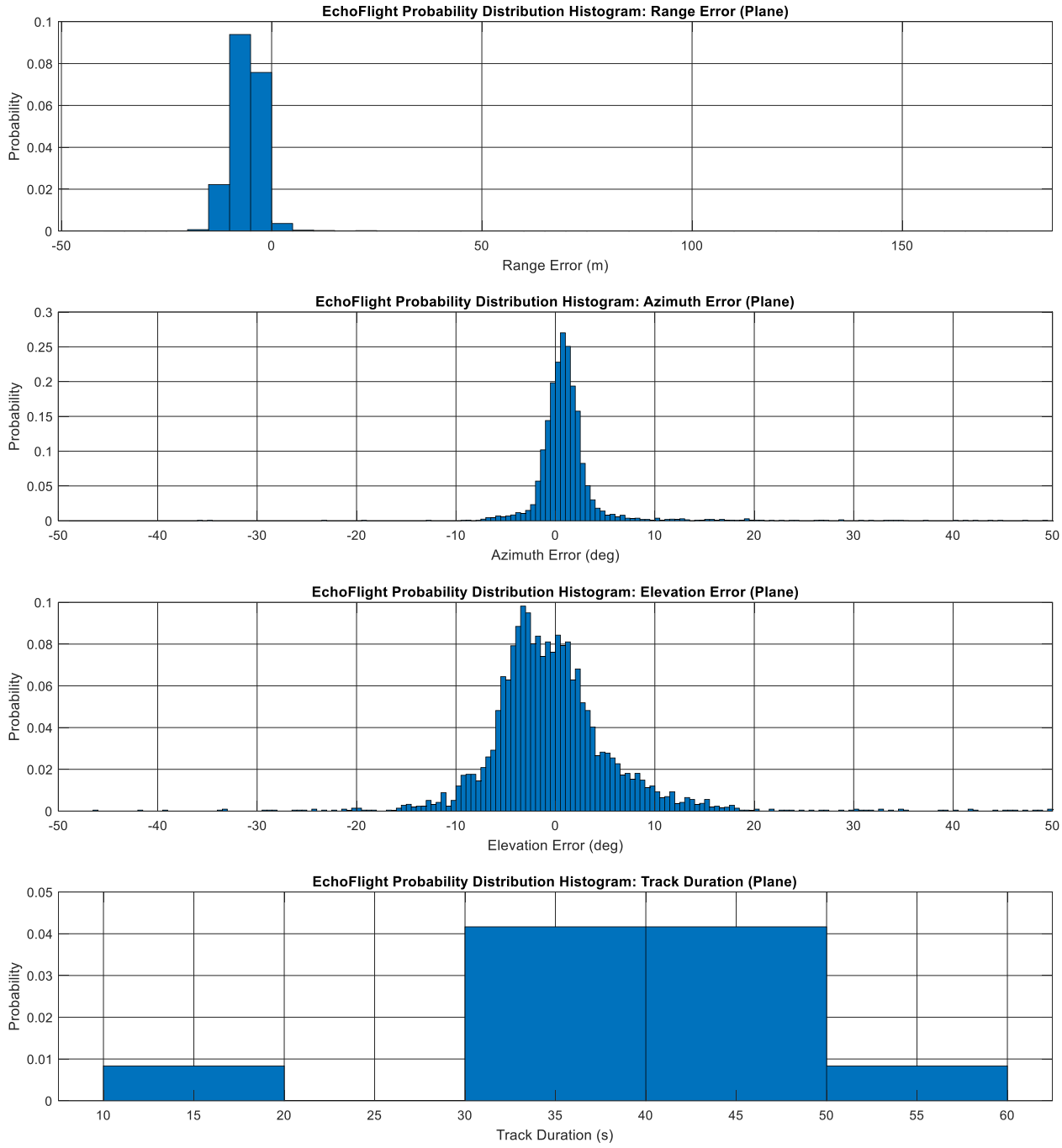

Figure 44: Error Probability Distribution Histograms (Plane)

8.1 Manufacturer's Comment (Paraphrased)

Echodyne was provided an advance copy of the results in Appendix C for comment. While no formal written response was received, the authors have paraphrased the comments received via e-mail correspondence and virtual meetings regarding the results presented in this section.

Echodyne identified several configuration settings that may have resulted in sub-optimal performance for the DAA application. In particular, they noted the following:

1. Several sorties were conducted with a -24 degree minimum elevation field of view which will result in added clutter. Efforts to reduce the clutter will also improve the track performance of airborne targets. Typically for airborne DAA applications a minimum elevation of -5 to -10 degrees is recommended.
2. The RCS mask was set wide at -30 to 100 dBsm, further increasing the likelihood of clutter. A value of -20 to +20 dBsm is recommended for airborne DAA applications. The Bell 206 appears to have an RCS of approximately +5 dBsm and the Harvard Mk IV is slightly higher than that, and a range of 0 to +10 dBsm would have been ideal for the flight trials. The authors note that for the purposes of these flight trials a conservative approach of accepting more false positives was adopted since the proper targets could be assessed in post-processing. It was felt that given the limited number of flight hours available that it was better to have increased false positives than to miss a true positive detection. The impact that this may have had on true track performance was not considered, however.
3. The AGL mask feature, which greatly reduces ground clutter, was not used. The authors note that in order to use the AGL mask feature effectively a boresighting and coordinate transform must be performed relative to the host aircraft's INS. Given the lever arm and angular rotation applied to the Echoflight's mounting location the authors were concerned that errors in calibration/measurement and coordinate transformation may have resulted in a reduction in the accuracy of the reported results.
4. Track minimum reporting confidence was left at the default value of 20%. Typically in DAA applications this would be set to 70% or more.
5. Track maximum confidence time was set to 1 second. When the priority is the minimization of false tracks this would typically be set to 2 seconds or more. This reduces the initial track range slightly as it takes more time after first detection to form a track, but also reduces the chances of false detections becoming tracks.

9.0 DATA ANALYSIS – FORTEM R20I

Due to the data connectivity issues described in section 5.3.2 and some flights having been conducted with inappropriate radar configuration parameters the track data from the R20i was not aligned with the manufacturers expectations nor previous flight test results. For this reason Fortem Technologies requested that the detailed results not be included as part of this publicly released report.

10.0 DISCUSSION AND CONCLUSIONS

DAA systems can be decomposed into two main functions, namely, (1) 'Detect' - situational awareness, determination and annunciation of traffic that may be in conflict; and (2) 'Avoid'—de-confliction maneuver execution, and determination of 'clear of conflict'. The 'Detect' function of a DAA system depends on sensor characteristics, e.g., signal-to-noise ratio of the target vs. background, false alarm rate, and processing/thresholding methods chosen, etc. The 'Avoid' function comprises the Remain Well Clear (RWC) and Collision Avoidance (CA) sub-functions, and depends on the RPA maneuvering characteristics, delays due to human factors (in the case if avoidance maneuver is not automatic), airspace specifics, and size of the protection volume. The RWC function assumes tactical maneuvers are performed within a timeframe nominally sufficient to coordinate with Air Traffic Control (ATC), whereas the CA sub-function is designed for urgent maneuvers performed as a last resort to prevent mid-air collisions when all other modes of separation fail.

In 2019, Transport Canada released Part IX of the Canadian Aviation Regulations, which provides a uniform set of regulations regarding RPAS operations conducted within Visual Line of Sight (VLOS).

While the current regulations have enabled greater commercial application of RPAS technology, the limitations imposed by the VLOS requirement prevent industry from fully harnessing the potential benefits of RPAS technology. To address this, TC has been working with numerous organisations to allow for limited-scope 'Low Risk' BVLOS operations, initially enabled through the issuance of a Special Flight Authorisation Certificate. In June 2023, TC published draft regulations in the Canada Gazette to enable Low-Risk BVLOS operations, public feedback was solicited and is being considered for potential amendments to the draft regulations. TC have drafted an Advisory Circular (AC) 903-001 (Reference 10) on RPAS Operational Risk Assessment, which follows the methodology described in the Joint Authority's on Rulemaking for Unmanned Systems (JARUS) Specific Operations Risk Assessment to provide Canadian RPAS operators with a structured process to assess the risks associated with RPAS operations, with a specific focus on BVLOS operations. As part of this process, the operator must determine the 'Risk Ratio', which is defined as the ability of the complete, 'end-to-end' DAA system to mitigate potential collisions with conflicting traffic.

Although the qualitative approach on how to assess a DAA system performance was outlined in AC 903-001, and in the SORA, a quantitative and agreed-upon approach to determine the Risk Ratio including a standard and test guide has yet to be published. At the time of writing, the Annexes presenting the supporting data for the SORA air risk model have yet to be published. Reference 11 presents a proposed approach that considers sensor performance, RPA maneuvering performance and airspace specifics. A key finding from this work is that the sensor performance alone is insufficient to establish the DAA risk ratio; one needs to consider the complete system including the integration with the aircraft and the airspace associated with the proposed operation.

The importance of flight testing DAA systems for RPAs cannot be overstated, as it is the ultimate validation of functionality and effectiveness of these systems in real-world scenarios, allowing both the operator and regulator to understand the degree to which DAA systems can mitigate the air risk. The airborne testing of three DAA sensors described in this report highlights the importance of flight testing for both system performance validation as well as system integration testing and development.

Both the EchoFlight and R20i required careful selection of operational parameters to achieve a desired balance between target sensitivity and clutter rejection. The testing described in this report did not assess the effects of parameter variation on critical performance characteristics such as range at first detection. There is a justifiable concern that a third-party integrator may 'over-tune' these systems to produce a minimum of false positives due to clutter at the expense of detection performance against real airborne threats. It is recommended that integrators perform representative flight testing (i.e. using a representative target aircraft and altitudes above ground level) to confirm that their tuning to reduce clutter effects still results in detections and tracks consistent with those required for the DAA risk ratio associated with the proposed operation.

None of the sensors tested can be considered as complete 'plug-and-play' systems. The task of having to integrate three sensors to a single airborne platform highlighted the fact that there is no common interface standard definition for DAA sensors. Moreover, the three sensors tested required different degrees of integration and levels of familiarity with the basic sensing modality and its associated parameters. Of the systems tested only the Casia X included collision threat detection and mitigation through the triggering of a pre-programmed maneuver such as 'descend and loiter'. The avoidance features of the Casia X were not tested as part of this project, however it is believed that a simulation study using representative detection ranges derived from the testing described here may be able to validate the efficacy of a pre-programmed avoidance maneuver. It is recommended that third part integrators conduct such simulation studies, with RPA maneuver characteristics validated by flight testing, as part of the process for establishing the total system risk ratio.

Integrators seeking to use the EchoFlight or R20i will need to implement their own threat detection module. Several techniques are identified in the literature such as the closest point of approach method of Reference 12, or the threat resolution module of ACAS-sXu (Reference 13). Note that while the Casia X did possess a threat detection module, Iris Automation did not specify the threat characteristics that result in the triggering of an automatic avoidance maneuver.

The challenges of system integration appear to be recognized by all three sensor manufacturers, as they each offered personalized assistance in the integration process. It is believed that such assistance is necessary, especially while these systems are still in the developmental stage and comprehensive integration guidance manuals have yet to be developed.

Both the Casia X and the EchoFlight rely upon position and orientation data as supplied from the host aircraft. Orientation errors from low cost/quality gyros as often found on small RPAs may be a cause for concern; as is the potential for calibration error between the host gyro and the camera. Moreover, there is a requirement for well established/documented 'boresighting' techniques to establish/verify the mechanical alignment between the host aircraft INS and the axis of the DAA sensor. This may be established in practice through the use of high quality (e.g. survey grade) GPS, and calibration targets (e.g. radar reflectors, or visual targets) at known orientations/distance from the sensor. The R20 featured an internal IMU and GPS receiver; making it unnecessary for the integrator to perform the georeferencing of the radar tracks. Analysis of the flight test data showed that georeferencing using the aircraft INS provided better results than the integrated IMU. It is speculated that this may have been a result of the high vibration environment of the Bell 205 saturating the IMU accelerometers. Further, low cost IMU systems often have drift issues in heading, particularly when hovering for extended periods.

There may exist opportunities to improve the tracking performance of the EchoFlight and R20i by using raw detections and a custom developed tracker that is intended for airborne targets such as an IMM tracker as described in References 14-17. The Casia X does not output raw detections, and since it uses estimation to establish range rather than direct measurement, it is less well served by the implementation of custom tracker in its current form.

All sensors exhibited average detection ranges that were comparable with the manufacturer's published specifications, however the variance between intercepts was significant. It is conjectured that this variance will have an impact on the realized risk ratio of the DAA system. A potential method to account for this effect was presented in Reference 11 through the use of cumulative probability of detection curves such as those shown in Figures 27 and 36 of this report. The range performance achieved for the closing rates tested yielded a time to closest approach of 20 to 40 seconds on average. These values are low if the decision making loop requires human intervention. If the DAA system requires human intervention, the delay times should be accounted for in any modelling effort used to assess the full system risk ratio.

The Casia X optical system exhibited comparable performance for range at first detection with both the helicopter and fixed wing target. Range estimation accuracy was reduced with the helicopter, however. The radars presented greater variability between the helicopter and fixed wing targets in terms of range at first detection with the helicopter being detected at a reduced range. It is suspected that this is indicative of the helicopter as having a lower observable RCS than the fixed wing aircraft.

All sensors exhibited worse elevation accuracy than azimuth across the testing performed. This is not surprising for the radars as radar sensor azimuthal and elevational accuracy are limited by beam size and antenna resolution, with elevation minimum resolvable angle typically being on the order of 3X the azimuthal resolution. The optical Casia X system, however, was expected to have equal accuracy in azimuth as elevation. It is uncertain as to where the source of this error resulted from. Nonetheless, the optical system showed greater azimuthal and elevational accuracy when compared to the radars, however it suffered in

range accuracy. This points to the potential benefits of fusing sensor modalities. In order for a sensor fusion approach to be viable the Casia X would need to output elevation and azimuth (and range) as opposed to the world referenced coordinate message that is presently used.

The salient conclusion from this flight testing is that the performance results are directly related to the quality of the system integration efforts. Moreover, one cannot conduct a performance assessment of the sensor alone without considering the integration into the greater system. This means that each integration of a DAA sensor into a specific RPAS and airspace (i.e. traffic distribution) will require a separate assessment of risk ratio, and supporting flight test validation. This highlights the need for a well established and agreed upon means for integrators to calculate the risk ratio such as the method proposed in Reference 11.

REFERENCES

1. K. Ellis, S. Jennings, “Test and Evaluation of the Seamatica Aerospace GuardianEye Ground Based Sense and Avoid System”, LTR-FRL-2019-0013, January 2019
2. K. Ellis, S. Jennings, C. El-Bouchi, “GuardianEye Phase 3B Flight Test Plan”, LTR-FRL-2018-0082, Nov 2018
3. K.Ellis, S. Jennings, P. Earle, “GuardianEye Phase 4 Flight Test Plan”, LTR-FRL-2018-0083, Nov 2018
4. K.Ellis, C. Paleske, S. Jennings, B. Carrothers, “Development and Flight Test of a Near Mid-Air Collision Intercept and Avoid Display”, LTR-FRL-2019-0063, July 2019
5. K. Ellis, I. Borshchova, “Transport Canada/LookNorth detect and avoid flight trials 202/2021”, LTR-FRL-2022-0098, November 2022, Transport Canada/LookNorth detect and avoid flight trials 2020/2021
6. K. Ellis, B. Gubbels, “Interface Control Document for NRC Bell 205 Ethernet Data System”, LTR-FRL-2014-0038, November 2015
7. B. Leach, J. Dillon, R. Rahbari, “Operational Experience with Optimal Integration of Low-Cost Inertial Sensors and GPS for Flight Test Requirements”, Canadian Aeronautics and Space Journal, June 2003
8. Anon, “GDL 90 Data Interface Specification” Garmin Ltd 560-1058-00 Rev A, June 5 2007, 560-1058-00A-GDL90_Public_ICD_RevA.doc (faa.gov)
9. K. Ellis, I. Borschova, S. Jennings, C. Paleske, “A comparison of two novel approaches for conducting detect and avoid flight test”, Journal of Unmanned Vehicle Systems, Vol 9, 2021
10. Remotely Piloted Aircraft Systems Task Force, AC 903-001; Remotely Piloted Aircraft Systems Operational Risk Assessment. Advisory Circular, Transport Canada, Civil Aviation, Ottawa, ON, Canada, 2021.
11. Ellis K, Borshchova I. Towards a Quantitative Approach for Determining DAA System Risk Ratio. Drones. 2023; 7(2):127. https://doi.org/10.3390/drones7020127
12. Iryna Borshchova and Kristopher Ellis. 2022. DAAMSIM: A simulation framework for establishing detect and avoid SYSTEM requirements. Drone Systems and Applications. 10(1): 266-286. https://doi.org/10.1139/dsa-2021-0044
13. L. E. Alvarez, I. Jessen, M. P. Owen, J. Silbermann and P. Wood, "ACAS sXu: Robust Decentralized Detect and Avoid for Small Unmanned Aircraft Systems," 2019 IEEE/AIAA 38th Digital Avionics Systems Conference (DASC), San Diego, CA, USA, 2019, pp. 1-9, doi: 10.1109/DASC43569.2019.9081631
14. G.A. Watson, W.D. Blair, “IMM Algorithm for tracking targets that maneuver through coordinated turn”, SPIE Proceedings 1698 Signal and Data Processing of Small Targets, 1992
15. R. Radhakrishnan, A. K. Singh, S. Bhaumik and N. K. Tomar, "IMM-cubature quadrature Kalman filter for manoeuvring target tracking," 2015 IEEE International Conference on Signal Processing, Informatics, Communication and Energy Systems (SPICES), Kozhikode, India, 2015, pp. 1-5, doi: 10.1109/SPICES.2015.7091498
16. Arroyo Cebeira A, Asensio Vicente M. Adaptive IMM-UKF for Airborne Tracking. Aerospace. 2023; 10(8):698. https://doi.org/10.3390/aerospace10080698